Summer 2016

Seismic anisotropy and mantle dynamics beneath the southeastern United States inferred from shear-wave splitting analysis

Yunhua Liu

Department:

SEISMIC ANISOTROPY AND MANTLE DYNAMICS BENEATH THE SOUTHEASTERN UNITED STATES INFERRED FROM SHEAR-WAVE SPLITTING ANALYSIS

by

YUNHUA LIU

A THESIS

Presented to the Faculty of the Graduate School of the

MISSOURI UNIVERSITY OF SCIENCE AND TECHNOLOGY

In Partial Fulfillment of the Requirements for the Degree

MASTER OF SCIENCE

in

GEOLOGY AND GEOPHYSICS

2016

Approved by

Stephen S. Gao, Advisor

Kelly H. Liu

Andreas Eckert

ABSTRACT

Systematic spatial variations of mantle azimuthal anisotropy are revealed by over 3000 pairs of high-quality shear-wave splitting parameters (fast polarization orientations and splitting times) recorded at ~400 USArray and other network stations in the SE United States (75˚-90˚ W, and 24˚-40˚ N). The fast polarization orientations observed in the continental interior are subparallel to the absolute plate motion (APM) direction of the North American plate with apparent larger-than-normal splitting times, indicating a significant asthenospheric contribution. Fast orientations parallel to the edge of the North American craton are revealed along the southern and eastern margins of the continent. A portion of the eastern coastal area shows weak anisotropy, probably indicating the existence of vertical mantle flow. The majority of the splitting measurements can be satisfactorily explained by a model involving simple shear in the boundary layer between the lithosphere and asthenosphere. The model includes three flow systems. The first is related to the continental scale APM-parallel relative movement between the lithosphere and asthenosphere which creates the APM-parallel fast orientations observed in the continental interior. The second flow system is associated with the deflection of asthenospheric flow around the edges of the craton and is responsible for the edge-parallel fast orientations observed along the southern and eastern margins of the study area. The third system is sub-vertical, possibly caused by vertically deflected flow along the eastern root of the craton, similar to the mechanism proposed by Refayee et al. (2014, doi: 10.1016/j.epsl.2013.01.031) for the western edge. It could also be related to previously proposed upwelling or down-welling flow.

ACKNOWLEDGEMENTS

My particular thanks to Dr. Stephen S. Gao and Dr. Kelly H. Liu, my advisors at Missouri University of Science and Technology, who introduce this study to me. Their spirits of assiduous study are worthy of respect. I learn to be a professional researcher from them. Notably, they provide ideas, guidance to my thesis. Without their suggestions and patience, this thesis would not have been completed.

I would like to express the sincere appreciation to my committee member, Dr. Andereas Eckert for his encouragement and advice in my thesis. I would also like to thank the Incorporated Research Institutions for Seismology Data Management Center for providing the seismic data in this study.

I am also grateful to Bin Yang and Fansheng Kong, my colleagues at the Missouri University of Science and Technology, who spent a lot of their valuable time to improve my thesis.

Last but not least, I would like to thank my father and mother. Without their unconditional support, love, and wishes, I would not able to do anything.

TABLE OF CONTENTS

LIST OF ILLUSTRATIONS

NOMENCLATURE

Symbol	Description
ϕ	Fast polarization orientation
δt	Splitting time

1. INTRODUCTION

1.1 SEISMIC ANISOTROPY

Shear-wave splitting (SWS) is the most powerful technique for studying seismic anisotropy, which is the consequence result of deformational processes beneath the Earth's surface in the lithosphere and asthenosphere [Silver, 1996; Savage, 1999]. SWS occurs when elastic waves travel through an anisotropic medium, in which the wave polarizing in one direction is faster than the other (Figure 1.1) [Savage, 1999].

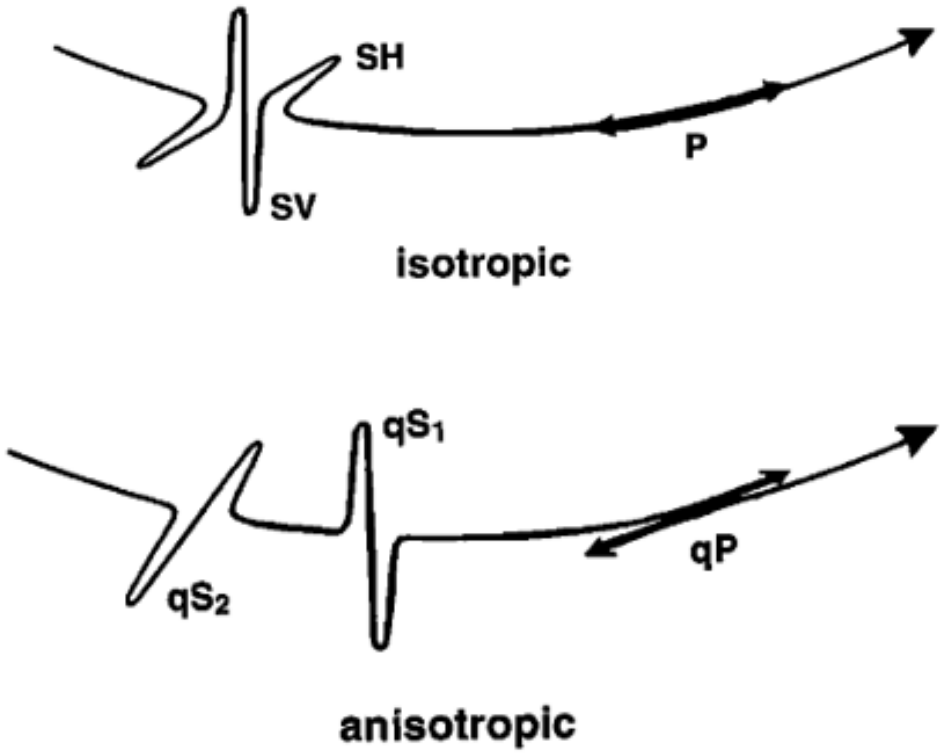

Figure 1.1 Three dimensional illustration of travel path in an anisotropic medium (upper plot) and an isotropic medium (bottom plot). In the isotropic medium, the P wave particle motion parallels to the propagation direction. The particle motion of S wave is perpendicular to propagation with SH (horizontal orientation) and SV (vertical plane). In the anisotropic medium, the qP wave particle motion is not parallel to the propagation direction. The qS waves are separated after traveled through the anisotropic medium [Savage, 1999].

Measurements of SWS provide two splitting parameters which are ϕ and δt. ϕ is the polarization orientation of the fast shear wave, and δt is the time delay between the slow and fast shear waves. These two parameters play decisive roles in the study of seismic anisotropy. Also, they are associated with mantle deformation and dynamics both in the lithosphere and asthenosphere [Silver and Chan, 1991].

P-to-S converted waves from the core-mantle boundary are most-commonly used in SWS studies. Those waves are collectively known as XKS, including SKS, SKKS, and PKS (Figure 1.2). At the core-mantle boundary (CMB) on the receiver side, they convert from P waves to S waves. Given the near-vertical ray path, shear wave splitting parameters have an outstanding lateral resolution but limited vertical resolution. Shear wave splitting could be caused by one or more layer of anisotropic medium along the wave path between the earthquakes and stations. Over the past several decades, many researchers have focused on determining where the splitting occurs along the path [Savage, 1999]. Laboratory and modeling studies indicate that lattice preferred orientation (LPO) of the olivine crystallographic axes is the major cause of shear wave splitting. Previous studies suggest that the fast orientation of anisotropic fabric is subparallel to the a-axis (Figure 1.3) of olivine [Zhang and Karato, 1995; Karato et al., 2008]. Under uniaxial compression, the shear waves with the highest propagating velocity polarize along a-axis of olivine (Figure 1.3), and the a-axis is perpendicular to the maximum compressional strain direction. Under pure shear, the a-axis is perpendicular to the shortening direction, while under simple shear, it aligns in the flow direction [Liu et al., 2008; Silver and Chan, 1991].

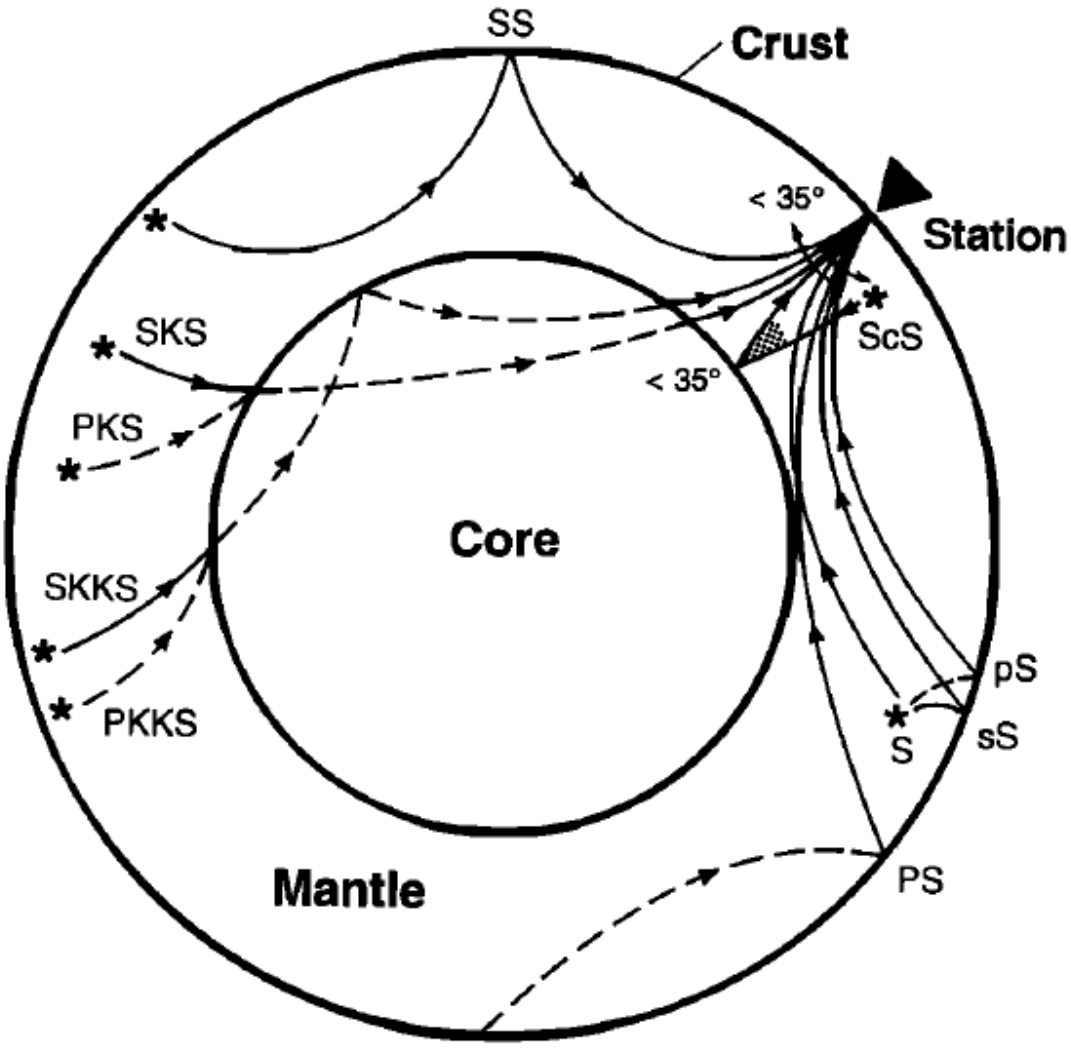

Figure 1.2 The three phases used for this study. Solid lines are S path segments, and dashed lines are P path segments. The stars are events, and the triangle represents the station [Savage, 1999].

The most pervasive factor causing seismic anisotropy is simple shear originated from flow gradient in the asthenosphere. This simple shear leads to the fast orientation parallel to the mantle flow direction, which in most cases parallels to the absolute plate motion (APM) direction of the plate (Figure 1.4). In the mantle, olivine is the most

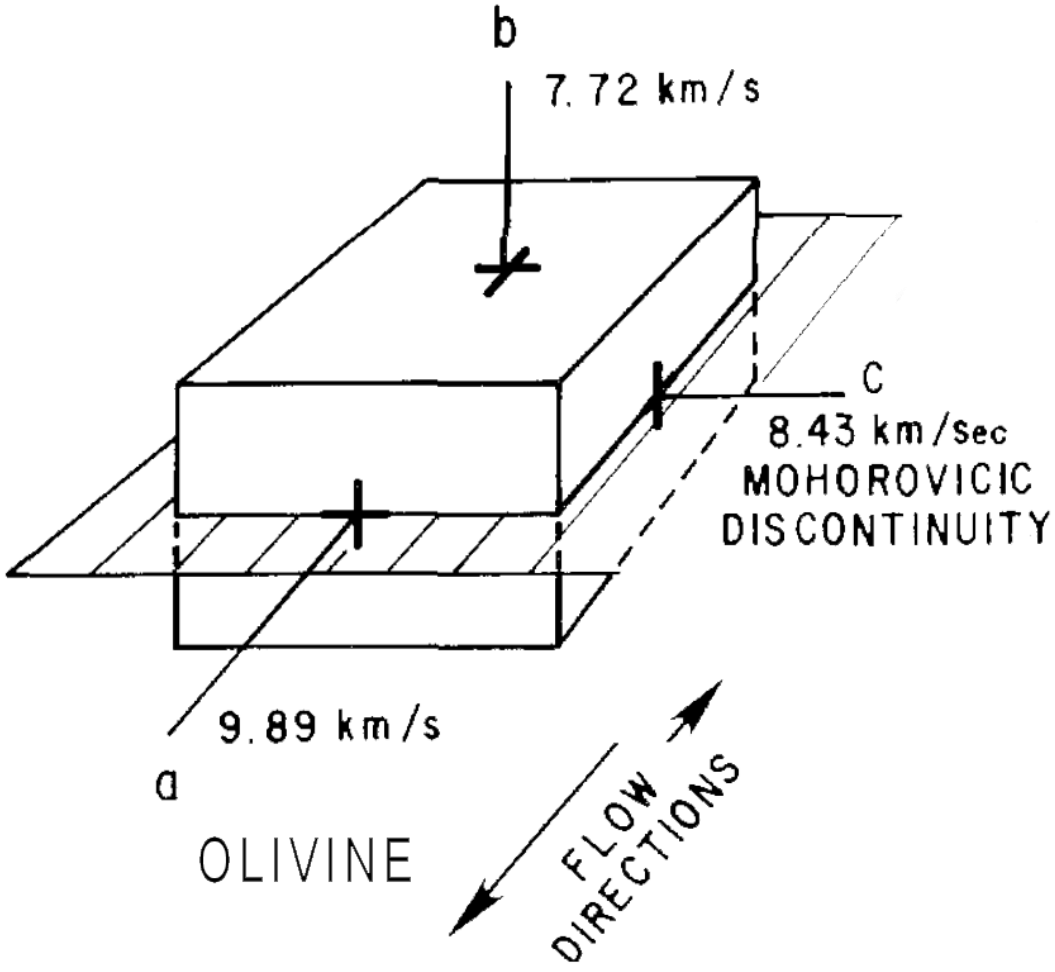

Figure 1.3 Shear wave velocities in an olivine crystal. The three unequal axes are orthogonal to each other. Seismic waves travel at different velocities in the direction of each of the axes. The fast orientation is subparallel to the a-axis which is also the flow direction [Anderson, 1989].

common anisotropic crystal. When olivine undergoes simple shear, the a-axis of the crystal is subparallel to the direction of shear. In such a case, the fast orientations parallel to the a-axis, which also parallels to the mantle flow direction.

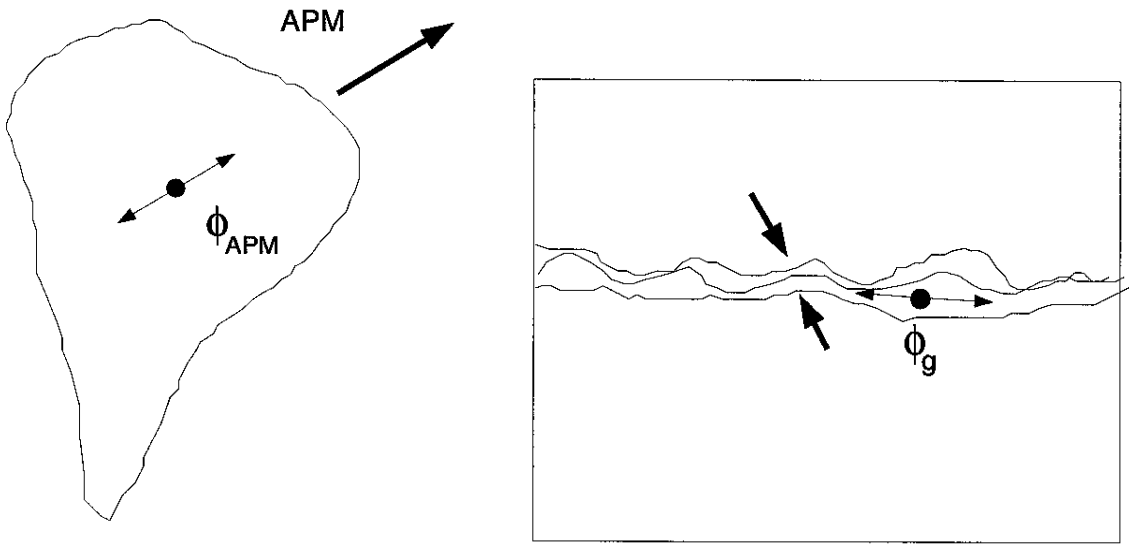

a)

Figure 1.4 Schematic of fast orientation corresponds to APM and deformation. a) The map view of a continent movement in APM direction and vertical coherent deformation for transpression. In the transpressional system, the bold arrow stands for convergence direction. The fast orientatio ϕ is parallel to the transpressional structure such as mountain belts. *b)* Cross-section view of simple asthenosphere flow. The lithosphere is moving by APM. The shade area is anisotropic layer concentrated with a-axis crystal, which causes ϕ parallel to the APM. *c)* The cross section view of vertical coherent deformation [Silver, 1996].

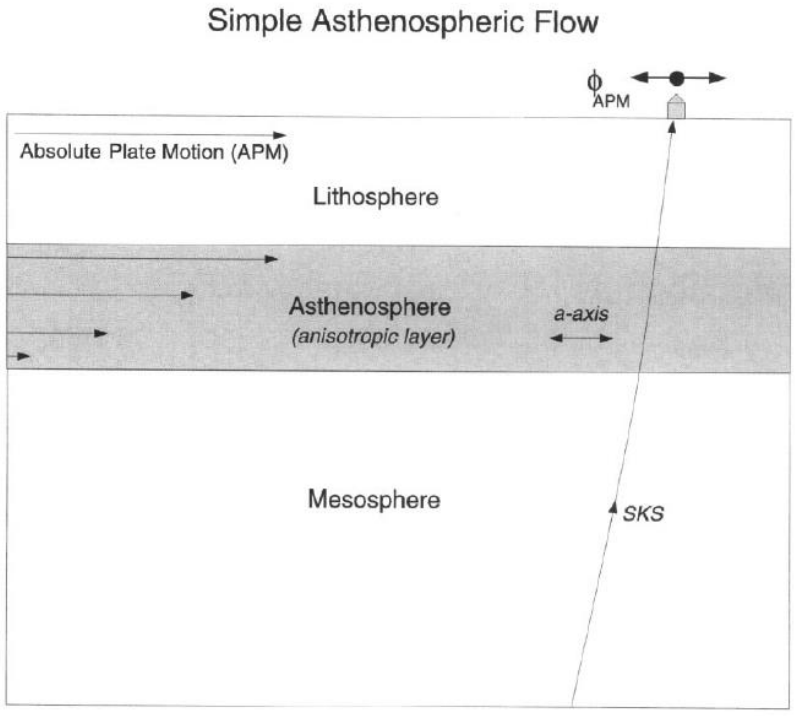

b)

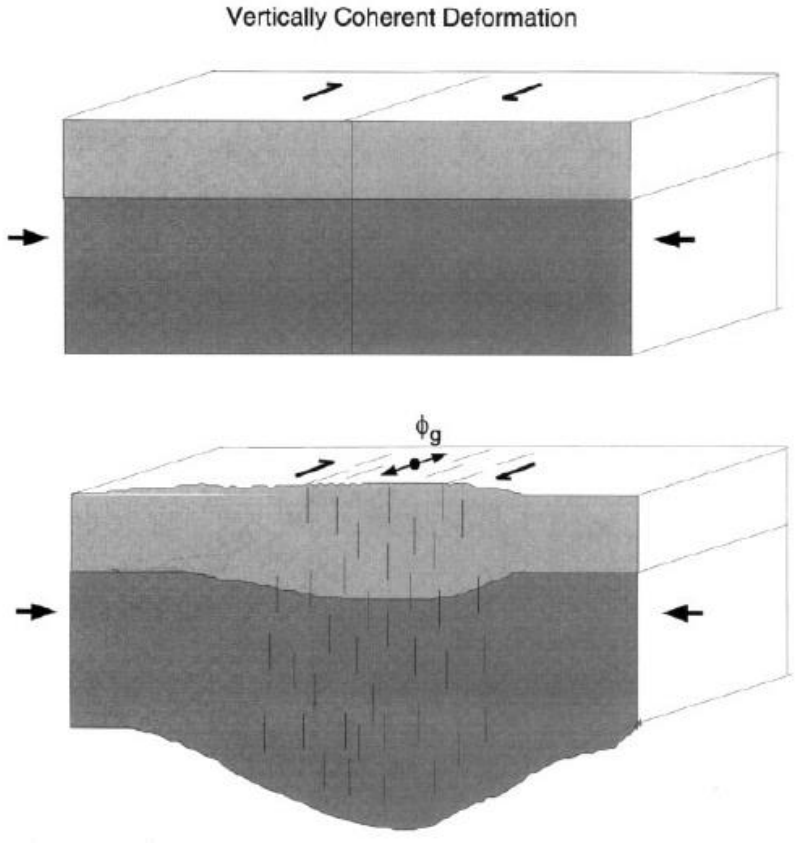

c)

Figure 1.4 (continued)

Besides mantle flow, lithospheric compression is also a predominant factor that can cause the anisotropy with the fast orientation parallel to the strike of the mountain belts (Figure 1.4) [Silver, 1996; Savage, 1999; Fouch and Rondenay, 2006; Long and Silver, 2009; Refayee et al., 2014].

1.2 TECTONIC SETTING AND PREVIOUS STUDIES

The southeastern North America has experienced an alternate geological history of extension and compression of continental margins involving successive terrane accretions, orogenies, and continent breakup. These tectonic processes could be summarized as two Wilson cycles of assembly and breakup of supercontinents (Figure 1.5) [Hoffman, 1991; Thomas, 2006; Cawood and Buchan, 2007; Hatcher, 2010]. There are three main tectonic provinces in southeastern North America, including the Yavapai (1.9-1.7 Ga), the Grenville (1.3-0.9 Ga), and the Appalachian (Figure 1.6) [Whitmeyer and Karlstrom, 2007]. The Appalachian formed during the Middle Ordovician to Permian. Regarding assembly of the Rodinia supercontinent, the ocean closed during 1350 Ma to 1000 Ma. At the same time, the Grenville orogeny formed [Hoffman, 1991]. The subsequent breakup of the Rodinia was accompanied by the opening of the Iapetus Ocean, and the isolation of the Laurentia. During the Permian closure of the Iapetus Ocean and assembly of the Pangaea supercontinent, the three orogenies including Taconic, Acadian, and Alleghania orogenies formed the Pangaea supercontinent and built

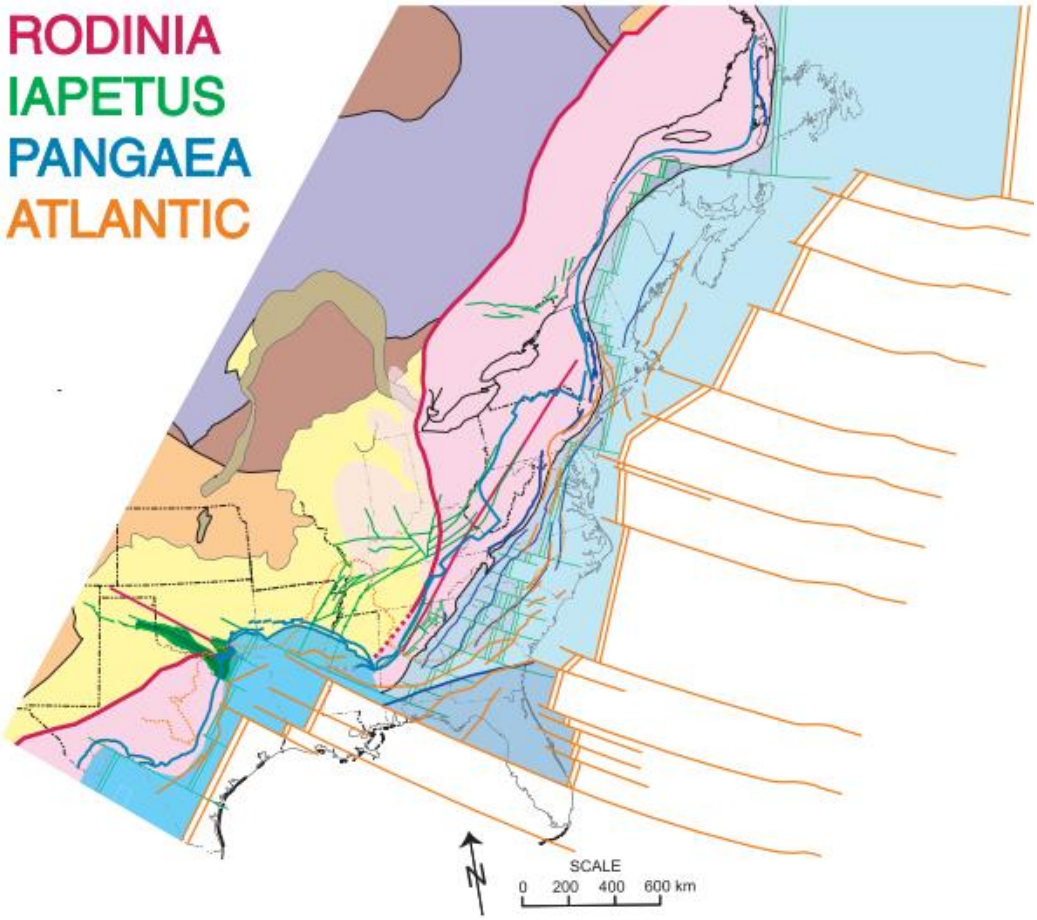

Figure 1.5 The Two complete Wilson cycles in eastern North America. Assembly of Rodinia, opening of the Iapetus Ocean, assembly of Pangaea, and opening of the Atlantic Ocean. Rodinia in red, Iapetus in green, Pangaea in blue, and Atlantic in orange [Thomas, 2006].

the Appalachian-Ouachita orogenic belt [Thomas, 2006]. The modern continental shelf and ocean floor document the breakup of Pangaea and the opening of the Atlantic Ocean.

Most previous XKS splitting studies in the eastern US revealed a pattern of fast orientations that are mostly sub-parallel to the APM directions [Barruol et al., 1997b; Fouch et al., 2000; Liu, 2009; Long et al., 2010]. Barruol et al. [1997b] noted that the APM-parallel fast orientations are also parallel to the local fabrics in the orogenic zone,

and interpreted the null splitting observations further east as being due to the intrusion of rifting-induced magmatism that would serve to weaken pre-existing fabrics.

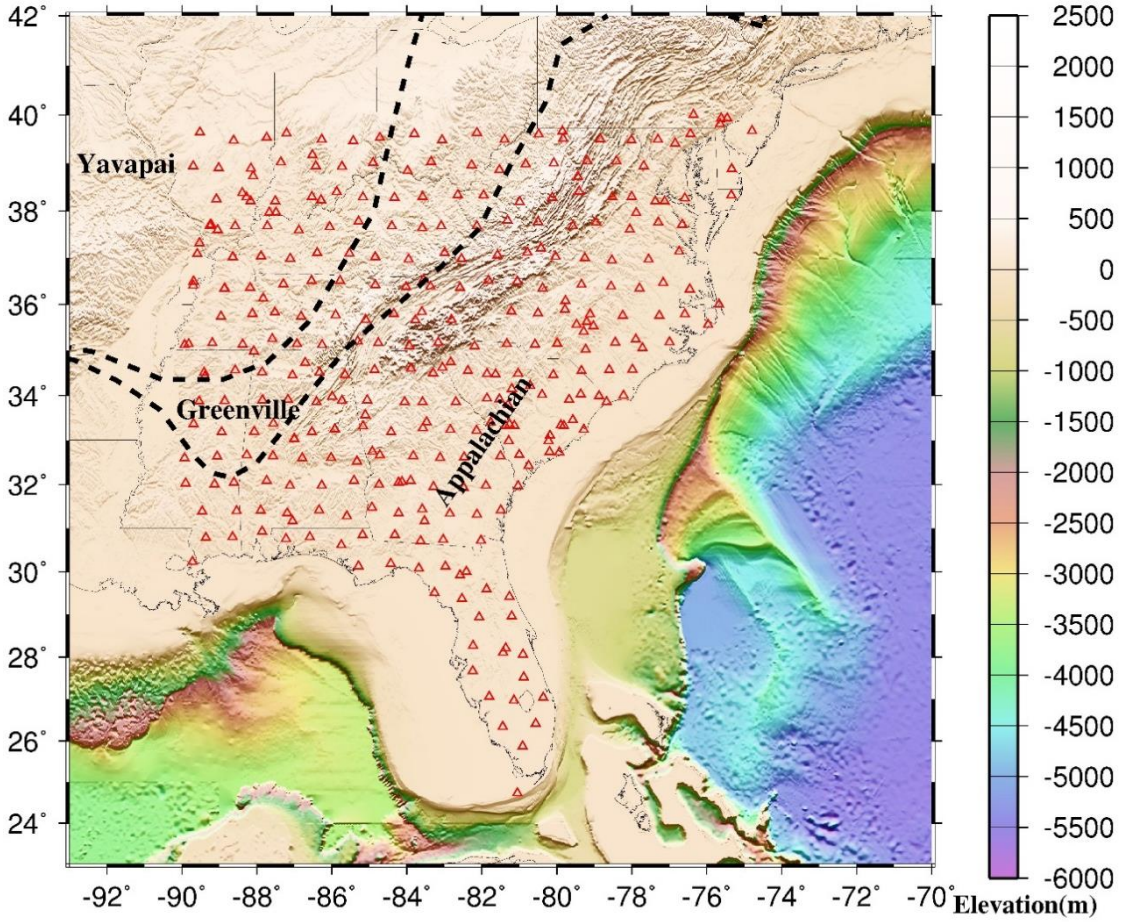

Figure 1.6. Map of stations used in this study. The red triangles are stations; the dash lines indicate the approximate boundaries of the Yavapai, Grenville, and Appalachian provinces.

Van der Lee et al. [2008] suggested a hydrous upwelling model associated with the dehydration of the Farallon slab. This vertical upwelling flow beneath the eastern North American margin is associated with surface uplift (Figure 1.7, left). They observed slow shear wave velocity anomaly in regional seismic waveform tomography beneath the eastern North America which parallel to the margin. King [2007] proposed that the

margin of eastern North America would be a likely point for edge-driven small-scale convection (Figure 1.7, right). This small-scale convection is produced by the sharp contrast between lithospheric thicknesses [King and Anderson, 1998].

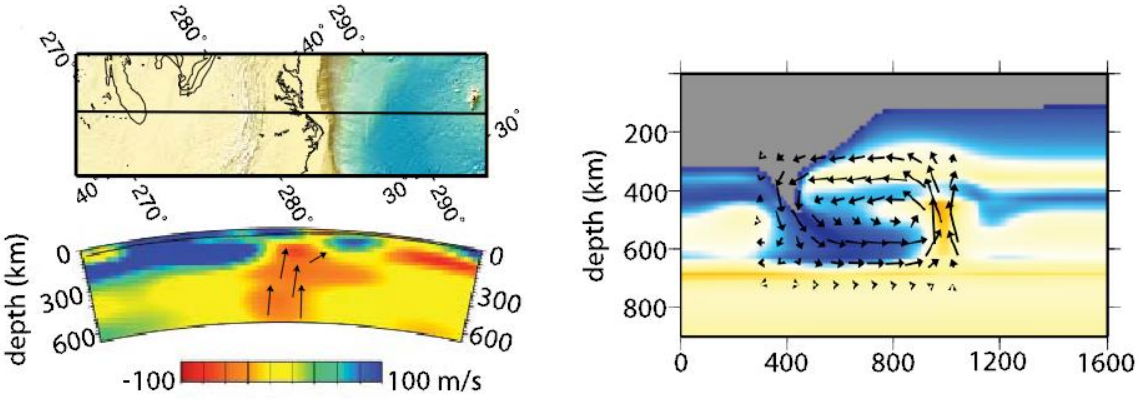

Figure 1.7 *(Left)* A slow shear wave velocity anomaly in the tomographic surface wave model NA04 [van der Lee and Frederiksen, 2005] beneath southeastern NA (map view). *(Right)* The predicted flow field from small-scale edge-driven convection is proposed by King and Anderson [1998].

Long et al. [2010] use SWS observations and receiver function analysis to test the proposed mantel flow geometries in the southeastern United States. SWS analysis show a contrast in splitting behavior between stations located on the continental interior, which tend to exhibit mainly NE-SW fast orientation with relatively large splitting time, and stations located closer to the coastal area, which are dominated by numerous null SKS splitting measurements. They support the vertical mantle flow model beneath the southeastern edge of the North American continent and APM-driven flow model beneath the continental interior. However, their receiver function analysis does not provide unambiguous evidence to support the hydrous upwelling model [Van der Lee et al., 2008] and the edge-driven convective downwelling model [King, 2007].

Wagner et al. [2012] also found that the fast orientations are roughly parallel to the APM of the North American plate within and west of the southern Appalachians, whereas to the southeast, many null splitting measurements are found over a range of back azimuths along with very few non-null measurements. They proposed that the difference in the splitting patterns was consistent with a transition from drag induced asthenospheric flow to vertical or incoherent mantle flow beneath the North American craton. In addition to these general patterns, they proposed that a number of non-null splitting measurements do not parallel to APM direction, but align with prominent magnetic anomalies that may correspond to continental suture zones or faults.

Long et al. [2015] proposed a limited correlation between the fast orientation and APM. They documented a pattern that the fast directions are parallel to the strike of the Appalachian mountain belts, suggesting a contribution from lithospheric deformation associated with the Appalachian orogeny. The area located in Virginia, North Carolina, South Carolina, and part of Georgia are dominated by null SKS measurements. The null measurements are consistent with the result in Long et al. [2010]. They proposed that these null measurements result from complex lithosphere structures, and near vertical mantle flow. In the Appalachian region, they observed fast orientations parallel to mountain strike, suggesting significant lithospheric contribution in this area. Overall, they proposed that upper mantle anisotropy beneath the eastern United States is complex, with likely contributions from both the asthenosphere and lithosphere in many regions.

2. DATA AND METHOD

2.1 DATA

The study area is located in the region with longitudes and latitudes ranging from 90°W - 55°W to 24°N - 40°N (Figure 1.6), respectively. This area is the southeastern part of the North American continent, mainly including the Appalachian mountain belts, Greenville orogeny, and Yavapai province.

The 2816 pairs of measurements were obtained from 418 events recorded by 382 stations within the southeastern North America. These broadband seismic data recorded by the USArray and other stations were requested from the Incorporated Research Institutions for Seismology (IRIS) Data Management Center (DMC). Figure 2.1 shows the distribution of the events that produced at least one well-defined measurement. The majority of the events are from the western Pacific and the Himalayas between the Indian and Eurasian plates. The azimuthal coverage of the events is outstanding for many stations, allowing a reliable detection of complex anisotropy. The seismograms obtained in this study were recorded during the period from 1993 to 2016. The splitting of P-to-S converted phases from the core-mantle boundary used in this study are PKS, SKKS, and SKS (collectively called XKS). The epicentral distances for PKS, SKKS, and SKS are 120°-180°, 95°-180°, and 84°-180°, respectively [Gao and Liu, 2009]. Notably, many previous studies only use the SKS phase. In contrast, in this study, we also use PKS and SKKS to maximize the lateral resolution and azimuthal coverage. The minimum magnitude is 5.6 for all events with the focal depth less than 100 km. If the focal depth is larger than 100 km, a lower cutoff magnitude of 5.5 is used to take the advantage of the sharper waveform.

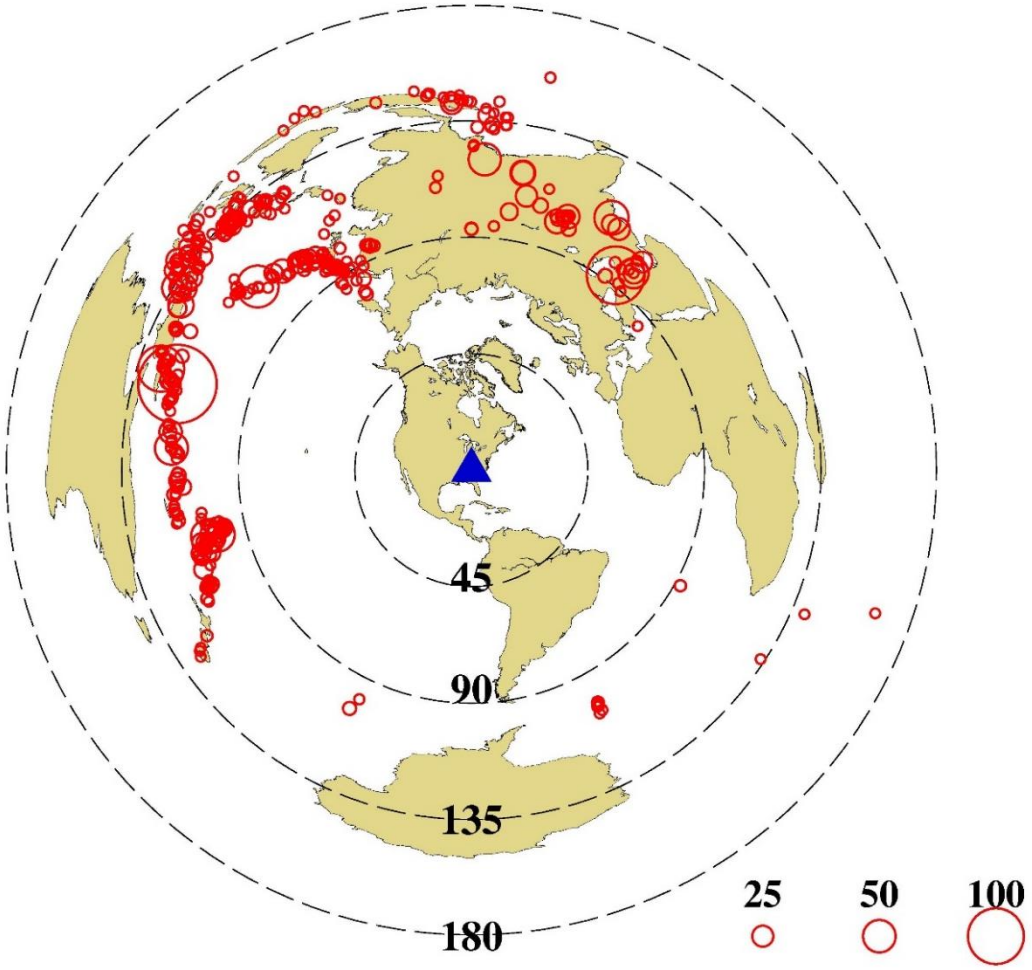

Figure 2.1 Azimuthal equidistant project map of the earth showing the distribution of earthquakes used in the study. The blue triangle is the center of the study area. The red circles denote the location of the epicenters of the earthquakes, and the size of red circles is proportional to the number of resulting well-defined splitting measurements.

2.2 METHOD

There are three commonly used SWS analysis techniques, including minimization of energy on the transverse component, minimization of eigenvalue of the covariance matrix, and maximization of cross-correlation between the resulting fast and slow

components [Silver and Chan, 1991; Savage and Silver, 1993]. When noise presents in the data, the minimization of transverse energy technique is the most stable one [Silver and Chan, 1991; Vecsey et al., 2008]. This method effectively removes the energy on the transverse component by grid searching for the optimal pair of splitting parameters. Once the optimal parameters are found, the fast and slow components are computed by rotating and time shifting the original radial and transverse components. The processed fast and slow components should have similar waveforms if the resulting parameters are reliable (Figure 2.3).

Following the procedures of measuring and ranking splitting parameters in Liu and Gao [2013] and Liu [2009] (Figure 2.2), which is based on the minimization of transverse energy method of Silver and Chan [1991], several steps which are the combination of automated processing and manual screening should be conducted.

At the first step, broad-band seismic data are requested from the IRIS DMC. The requested traces start from 100 s before the theoretical arrival time of the first compressional wave and are 1100 s long [Liu and Gao, 2013]. Each seismogram may contain all the three XKS phases in different time windows. The second step is data selection: The raw data requested from the IRIS DMC are converted into Seismic Analysis Codes (SAC) format, and resampled into a uniform sampling rate of 20 samples per second. The SAC files are band-pass filtered in the frequency band of 0.04-0.5 Hz, which contains most of the XKS energy. The horizontal N-S, and E-W components are then rotated to radial and transverse components. An automatic trace selection procedure

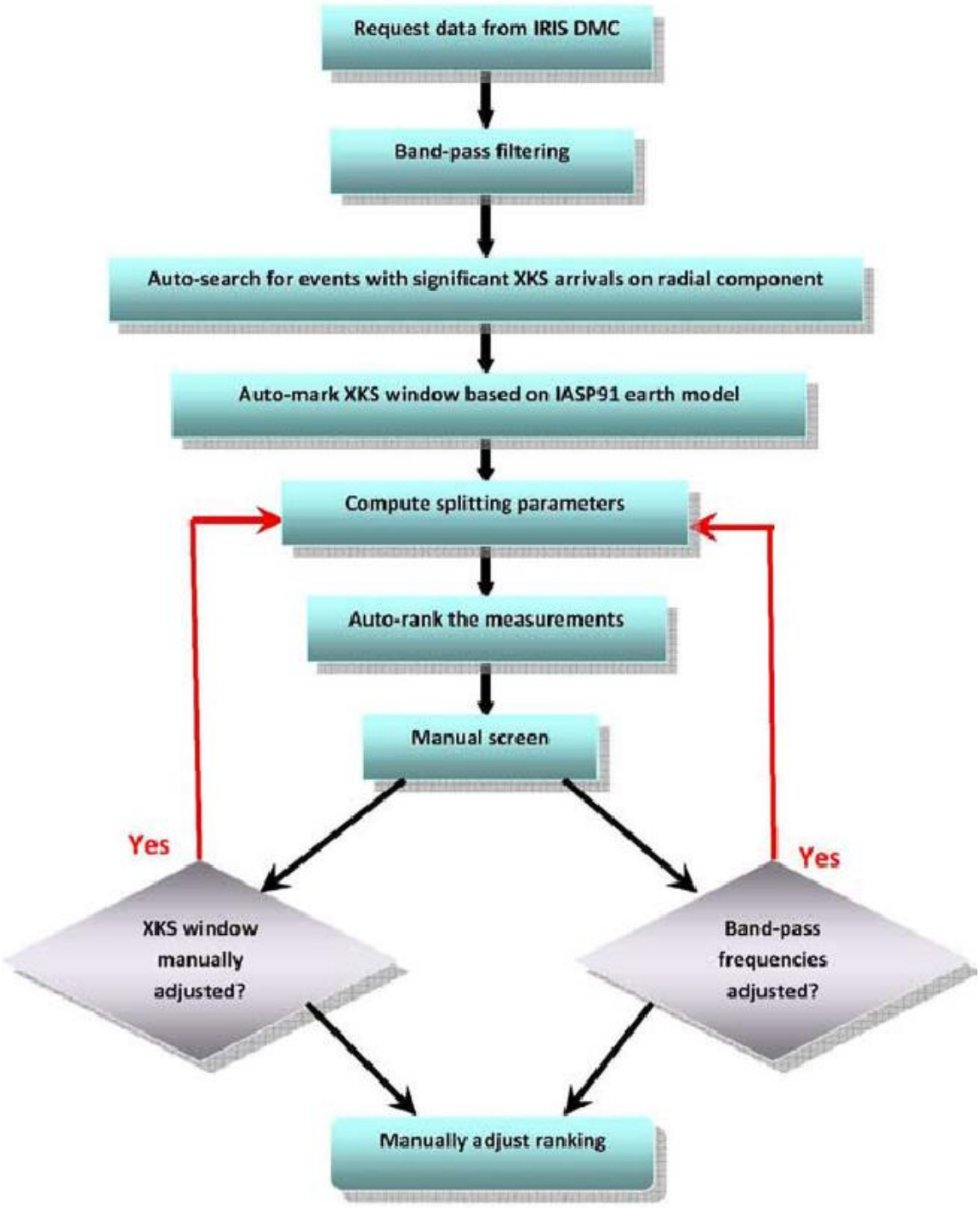

Figure 2.2 A flowchart displaying the main procedure for measuring, verifying, and ranking shear wave splitting parameters for making reliable SWS measurements [Liu, 2009].

is then applied to reject low signal-noise-ratio (SNR) measurements on the radial component. After the event selection procedure, 40% of the SKS and 30% of the PKS and SKKS seismograms were kept. For the third step, all accepted measurements are automatically ranked based on SNR in the original radial, original transverse, and corrected transverse components [Liu et al., 2008; Liu and Gao, 2013].

The measurements are automatically ranked into five qualities: A, B, C, N, and S. Quality A and B measurements have significant XKS arrivals on both the original radial and transverse components, and near perfect removal of XKS energy on the corrected transverse component. Quality C measurements have low energy on the original radial component, and are not used in the study. The null measurements, which are ranked as N, have significant XKS arrivals on the original radial component but no XKS arrivals on the original transverse component. The Quality S measurements have outstanding XKS arrivals on both the original radial and transverse components. However, on the corrected transverse components the XKS energy cannot be effectively removed. Once the automatic processing is done, careful manual verification and adjustments to the data-processing parameters are applied to produce reliable SWS measurements [Liu and Gao, 2013].

Manual screening is based on three steps which are adjusting the start and end times of XKS arrivals, adjusting the filtering parameters, and quality ranking.

The first step is changing the XKS window to exclude non-XKS arrivals and reduce the standard deviation of the measurements (see Figure 2.3 for an example) by moving the two boundaries on the each side of XKS arrivals. If the XKS arrivals have some low-frequency noises, bandpass filtering frequencies should be adjusted. Once the

adjusting is settled, the quality ranking might be altered. The procedure is demonstrated by the examples showing in Figures 2.4-2.9.

Rank A is given only if the measurements have the four features described as follow. First, strong XKS arrivals are displayed on both the original radial and transverse components (Figure 2.3a). Second, almost all the XKS energy on the corrected transverse component is removed effectively. Third, the original particle motion pattern is elliptical, and the corrected particle motion pattern is close to linear (Figure 2.3c). Fourth, a single significant point is found corresponding to the lowest energy in the contour map (Figure 2.3d). Quality B measurements (Figures 2.6 and 2.7) have slightly lower quality than A (Figures 2.4 and 2.5). Both Quality A and Quality B measurements will be used for analysis. Quality C measurements are dominated by low energy on the original radial and/or transverse component and are not used. For Quality C measurements, the similarity between the fast and slow waveforms is low, and the particle motion pattern of the corrected component is non-linear, and/or the original particle motion pattern of the original component is non-elliptical. The standard deviation of the measurements is high, up to the 22.5° for ϕ which is the largest possible value. If strong energy is displayed on the radial component but low energy on the original transverse component, these measurements are ranked as Quality N (Figures 2.8 and 2.9).

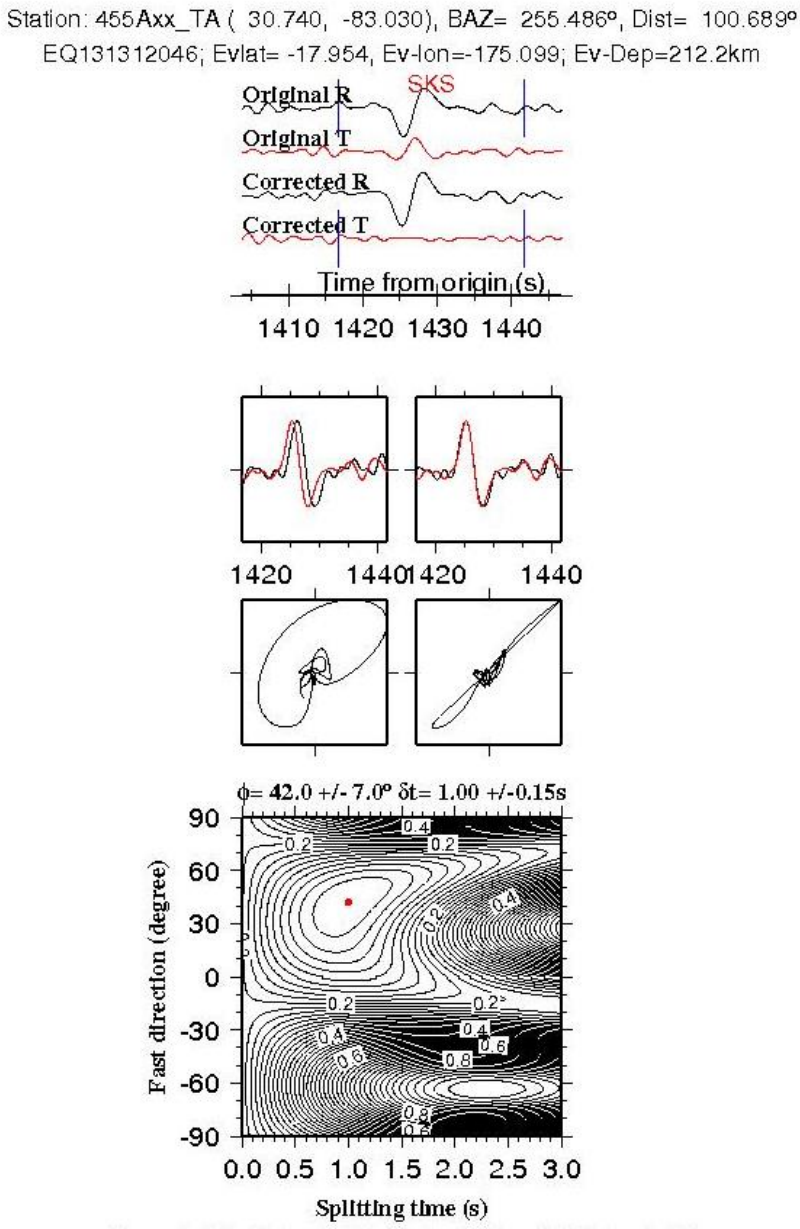

Figure 2.3 Diagrams of SWS measurements at station 455A. (a) Original radial, original transverse, corrected radial, and corrected transverse components. The section between the two vertical bars is the XKS window used for SWS analysis. Shown on top are station and event names and locations. (b) The left plot shows resulting fast (dashed) and slow (solid) components, and in the right plot the slow component is advanced by the optimal splitting time. (c) Particle motion patterns for the original fast and slow (left) and shifted fast and slow (right) components shown in (b). (d) Contour of energy on the corrected transverse component as a function of trial fast orientations and splitting times. The red dot indicates the optimal splitting parameters corresponding to the minimum energy.

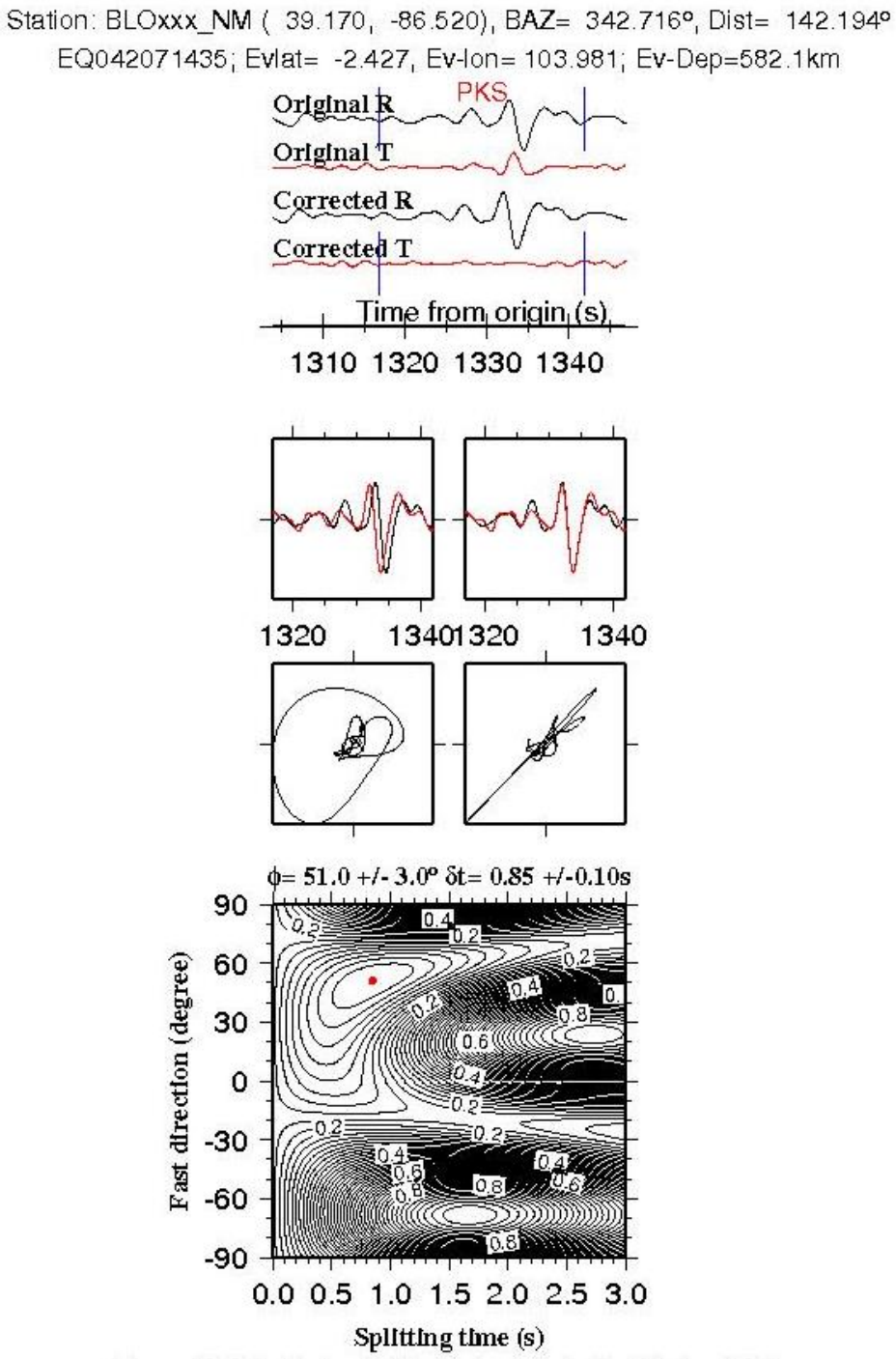

Figure 2.4 Quality A example of PKS measurements from station BLO_NM in the Yavapai province.

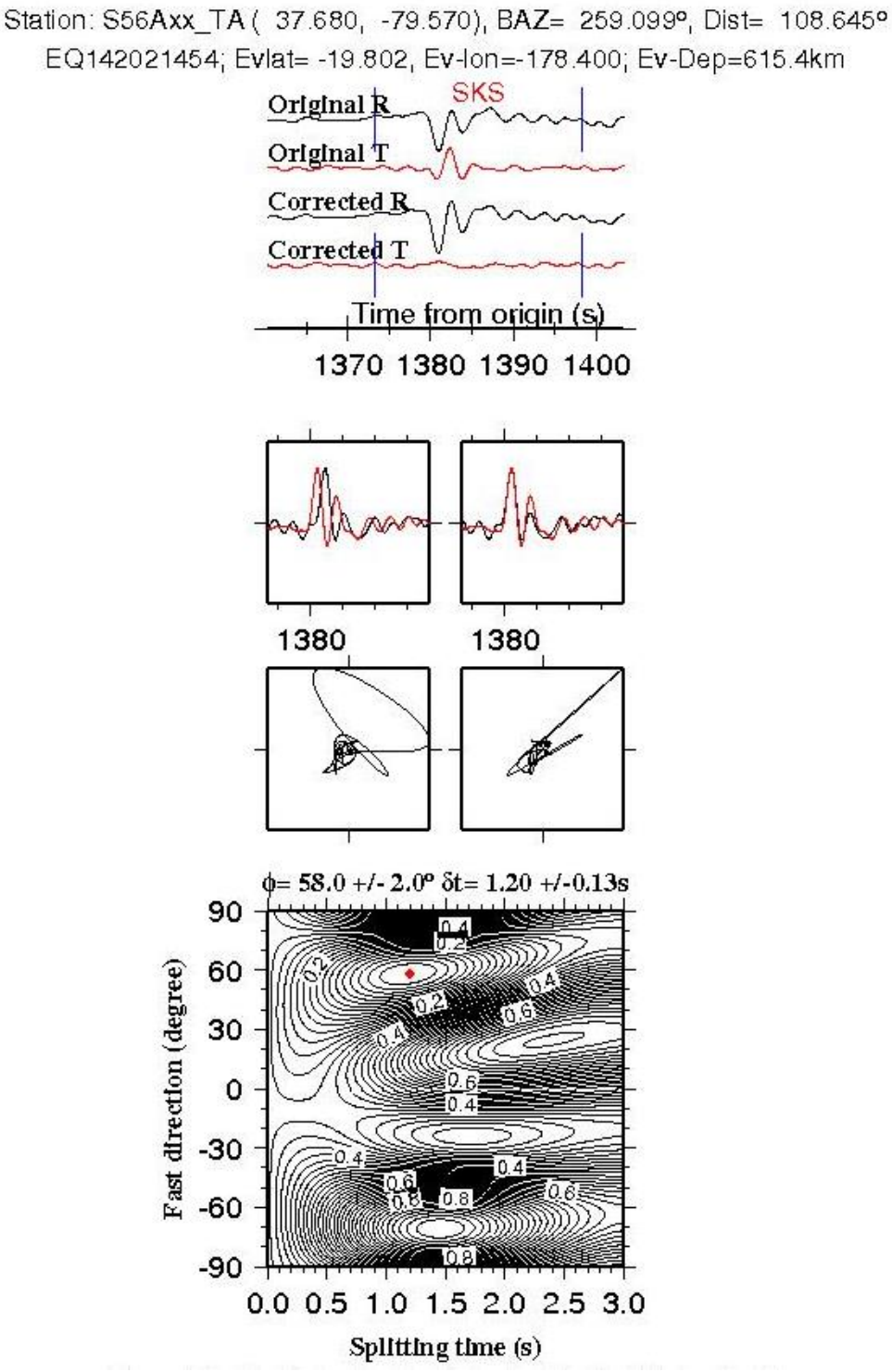

Figure 2.5 Quality A example of SKS measurements from station S56A in the Appalachian province.

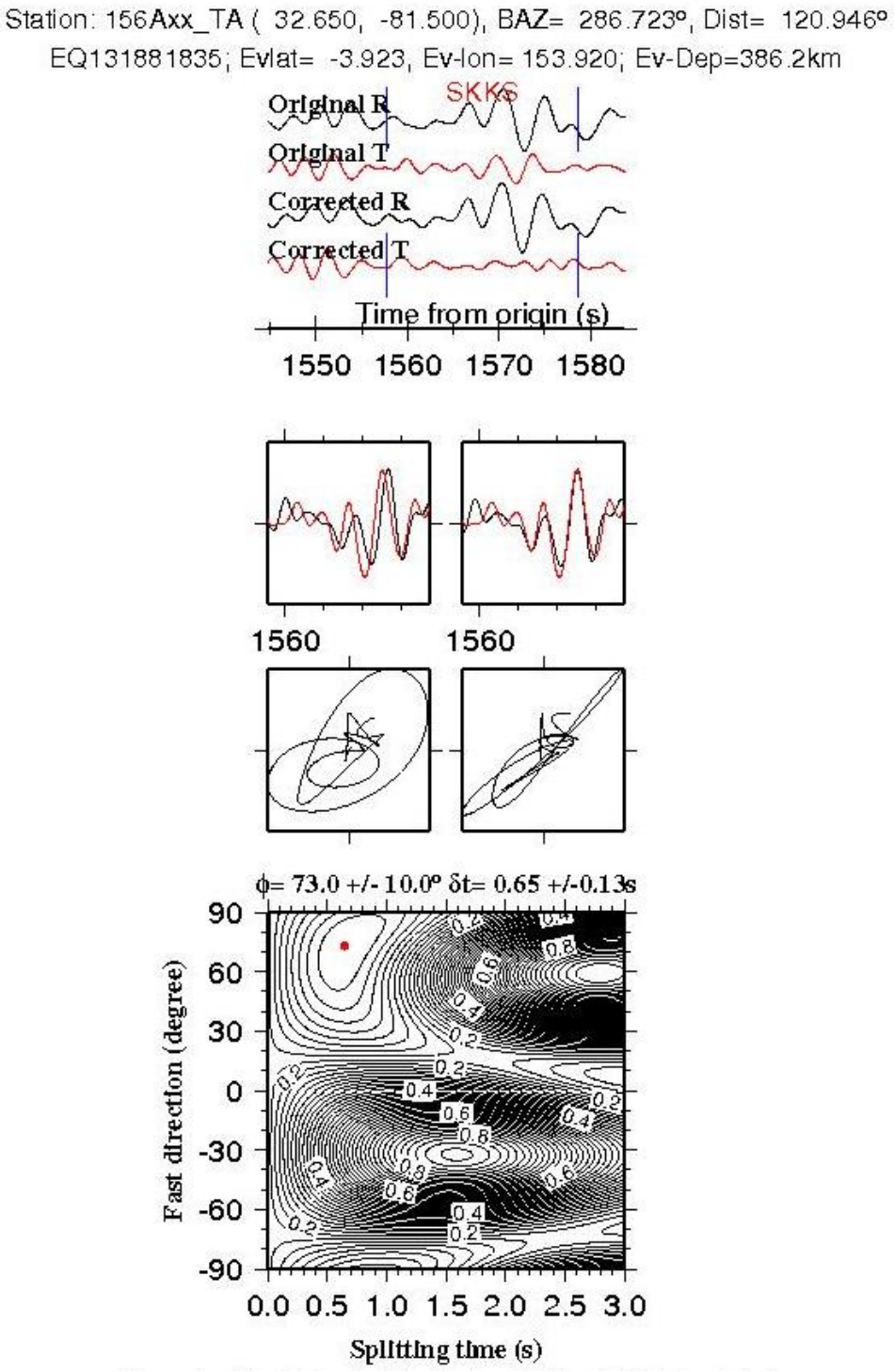

Figure 2.6 Quality B example of SKKS measurements from station 156A in the Appalachian province.

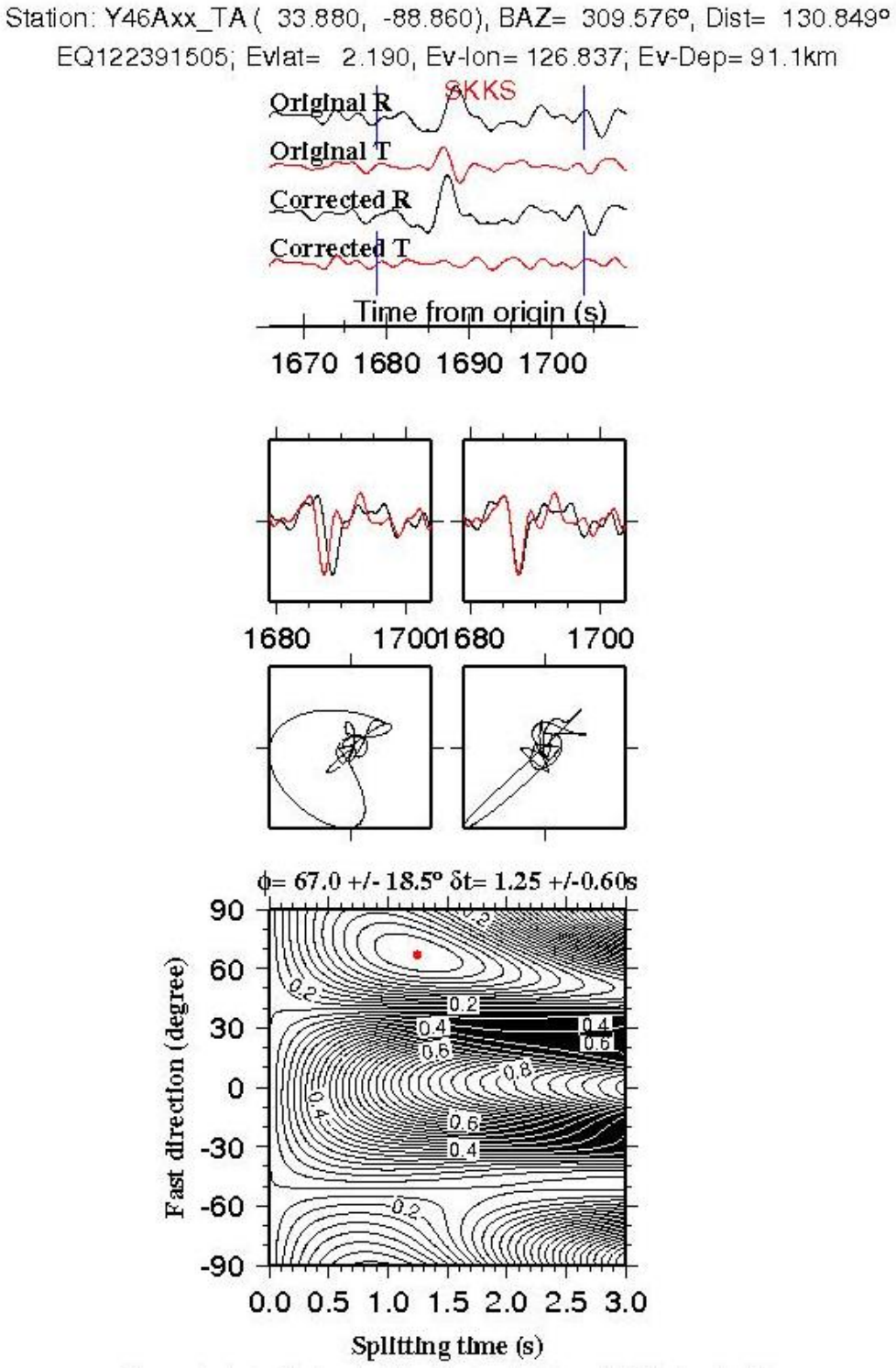

Figure 2.7 Quality B example of SKKS measurements from station Y46A in the Greenville province.

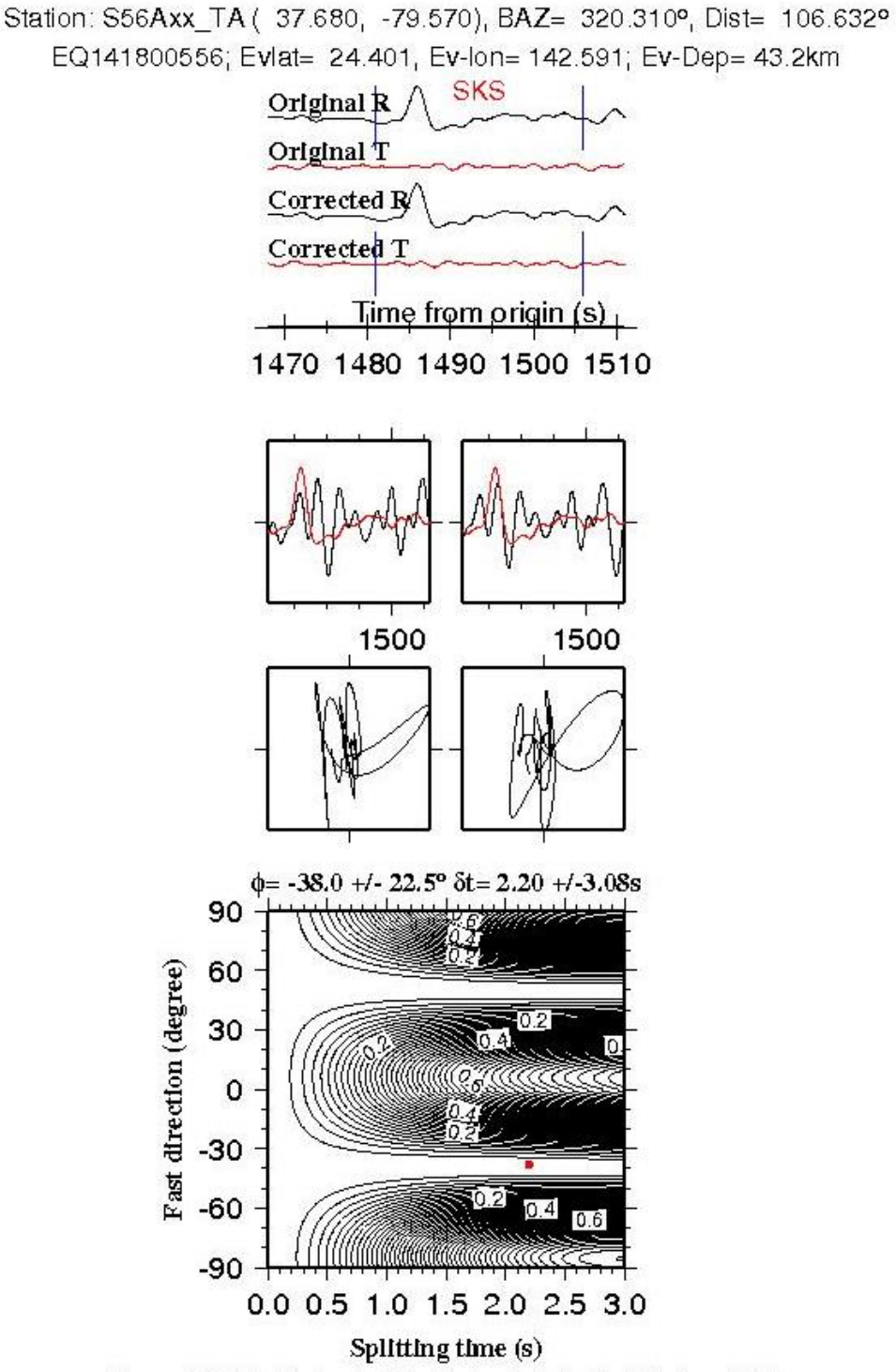

Figure 2.8 A Quality N example of SKS measurements from station S56A in the Appalachian province.

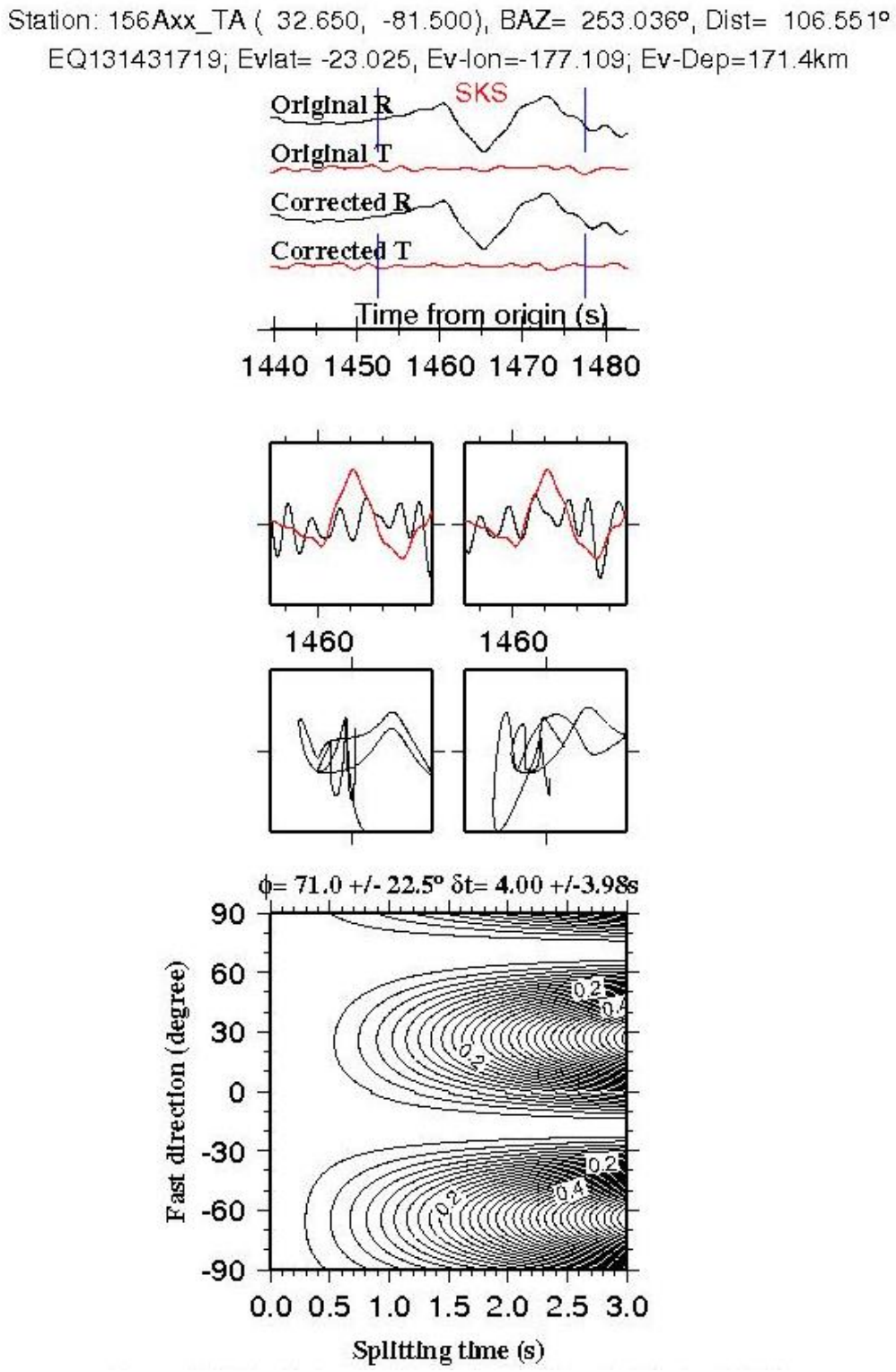

Figure 2.9 A Quality N example of SKS measurements from station 156A in the Appalachian province.

To locate the anisotropic medium, Liu and Gao [2011] proposed a procedure to estimate the depth of the source of anisotropy using the spatial variation of splitting parameters. This technique requires the availability of high-quality SWS measurements obtained at densely spaced seismic stations. From the previous studies [Montagner, 1998; Yuan and Romanowicz, 2010], the surface wave dispersion studies can also resolve the depth distribution of seismic anisotropy, but the resolution in both the vertical and horizontal directions is intrinsically low.

3. RESULTS

3.1 GENERAL RESULTS OF SPLITTING PARAMETERS

The data processing and manually checking resulted in a total of 2816 pairs of well-defined (Quality A and B) splitting parameters recorded by 382 stations. The dataset includes 619 PKS, 480 SKKS and 1718 SKS measurements (Figure 3.1). Examples of SWS measurements are shown in Figures 2.3-2.9. The mean value of the delay times over all the measurements is 0.95±0.29 s, which is close to the global average of 1.0 s for the continents [Silver, 1996].To facilitate the interpretation of the resulting SWS parameters and comparison of the fast orientations with the geological features, the study area is divided into three parts based major geological boundaries.

The Yavapai province contains 866 pairs of measurements from 76 stations with the mean splitting time of 0.92±0.28 s and mean fast orientation of 64.1 °±20.9 °. The fast measured orientation generally trend NE-SW in the Yavapai province, while the trend is close to E-W in the vicinity of the New Madrid seismic zone.

The Greenville province is composed of 432 measurements from 51 stations. The mean fast orientation is 56.1 °±17.1 °. The fast orientations are NE-SW in the northeastern portion of the Grenville province, which is consistent with the vicinity of Yavapai. However, there is a slight change in the fast orientations in the southern portion of the Grenville from NE-SW to E-W. The mean splitting time for this area is 0.99±0.29s.

The 1595 measurements from 255 stations in the Appalachian province have a mean fast orientation of 68.7 °±23.6 ° and a mean splitting time of 0.95±0.29 s. In this

area the patterns of the fast orientations and splitting times are complex. In the Appalachian orogeny, the fast orientations are subparallel to the strike of the mountain belts which is approximately in the NE-SW direction. The fast orientations are parallel to the continental margin at the northern and southeastern portions of the study area.

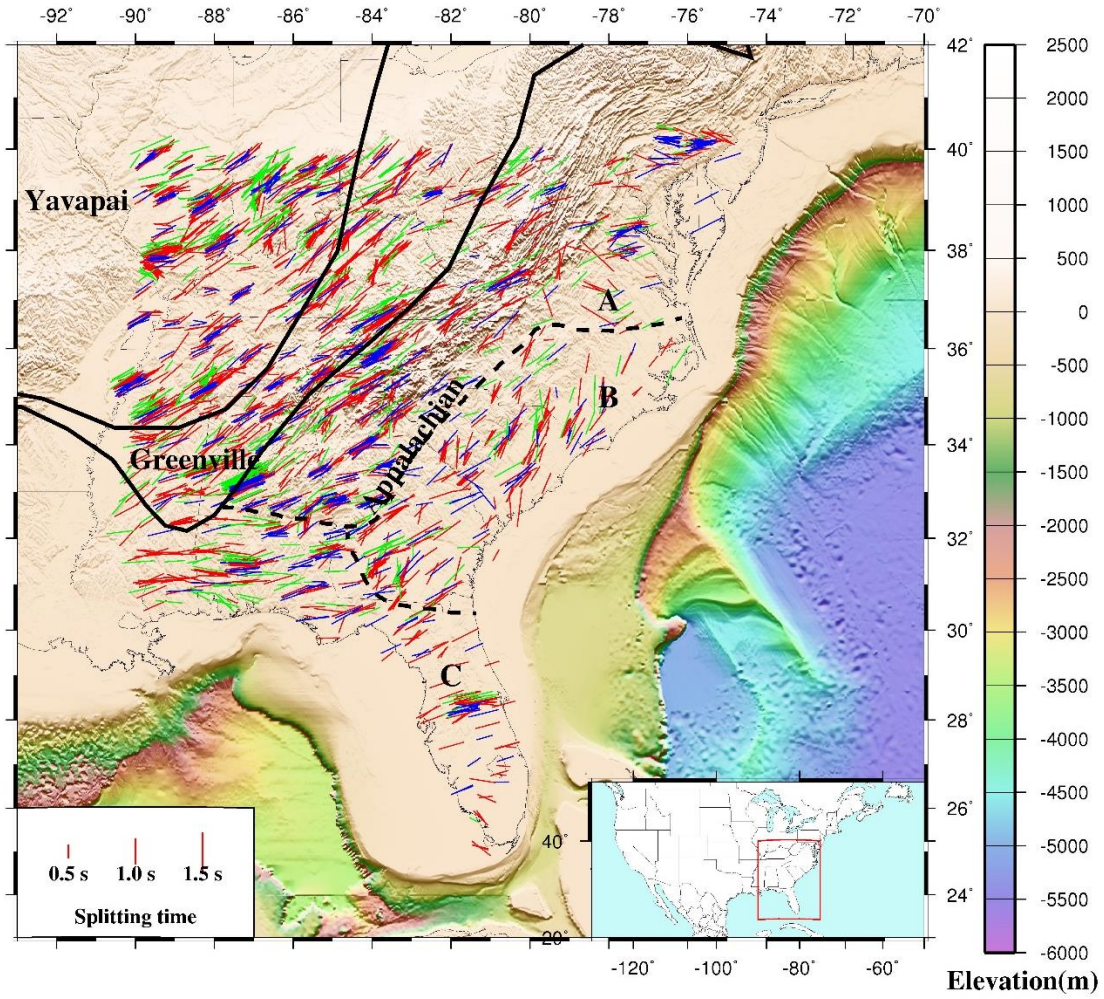

Figure 3.1 Resulting SWS measurements plotted above 200 km ray-piercing points. XKS measurements are denoted in different colors: blue for PKS, green for SKKS, and red for SKS. The length of each line is proportional to the duration of δt, and the orientation of each line corresponds to ϕ. The solid lines divide the study area into three parts based on the geological province [Hoffman, 1988] which are the Yavapai province, Greenville province, and the Appalachian province. The dash line are boundaries of three region of the Appalachian province. The small inset map of study area is located at the lower-right corner of the figure.

3.2 SPATIAL VARIATIONS OF THE RESULTING SPLITTING PARAMETERS IN THE APPALACHIAN PROVINCE

In the Appalachian province, the SWS measurements have more complex patterns in the fast orientations and splitting times than other areas. Consequently, this area is divided into three smaller areas based upon the trend of fast orientation to better explore the origin of the observed anisotropy. Area A is assigned in the Appalachian mountain belt (Figure 3.1), in which the fast orientations generally trend NE-SW, which are roughly parallel to the strike of the orogeny. The pattern of fast orientation slightly changed in the eastern portion of area A. The average polarization orientation is 63.4°±19.7° and the average splitting time is 0.95 ± 0.30 s from 849 measurements observed at 105 stations. This is consistent with the previous studies [Long et al., 2010, Wagner et al., 2012, Long et al., 2015]. Area B located at the eastern coastal area has a large quality of different fast orientations than areas A and C. The 345 measurements from 84 stations have an averaged fast orientation of 39.5°±24.1° and an averaged splitting time of 0.87±0.26 s. There is a notable rotation of the fast orientations between the western portion of area C and area B from nearly E-W to generally NNE-SSW. Area C is the southern part of the Appalachian province which contains 348 pairs of SWS measurements from 62 stations. The mean fast orientation is 80.3°±16.8° and the mean splitting time is 1.02 ± 0.27 s.

3.3 RELATIONSHIP BETWEEN THE FAST ORIENTATIONS AND THE APM

To explore the relationship between the spatial variation of the fast orientations and APM direction, the absolute difference of these two values is calculated in the range of 0° to 90° for each of the 2816 ray-piercing points at the depth of 200 km. The APM

direction is based on the model of Gripp and Gordon [2002]. The resulting differences (Figure 3.2) are then spatially resampled in 1° × 1° overlaying blocks with a moving step of 0.05°. The result indicates that the fast orientations in the Yavapai province are

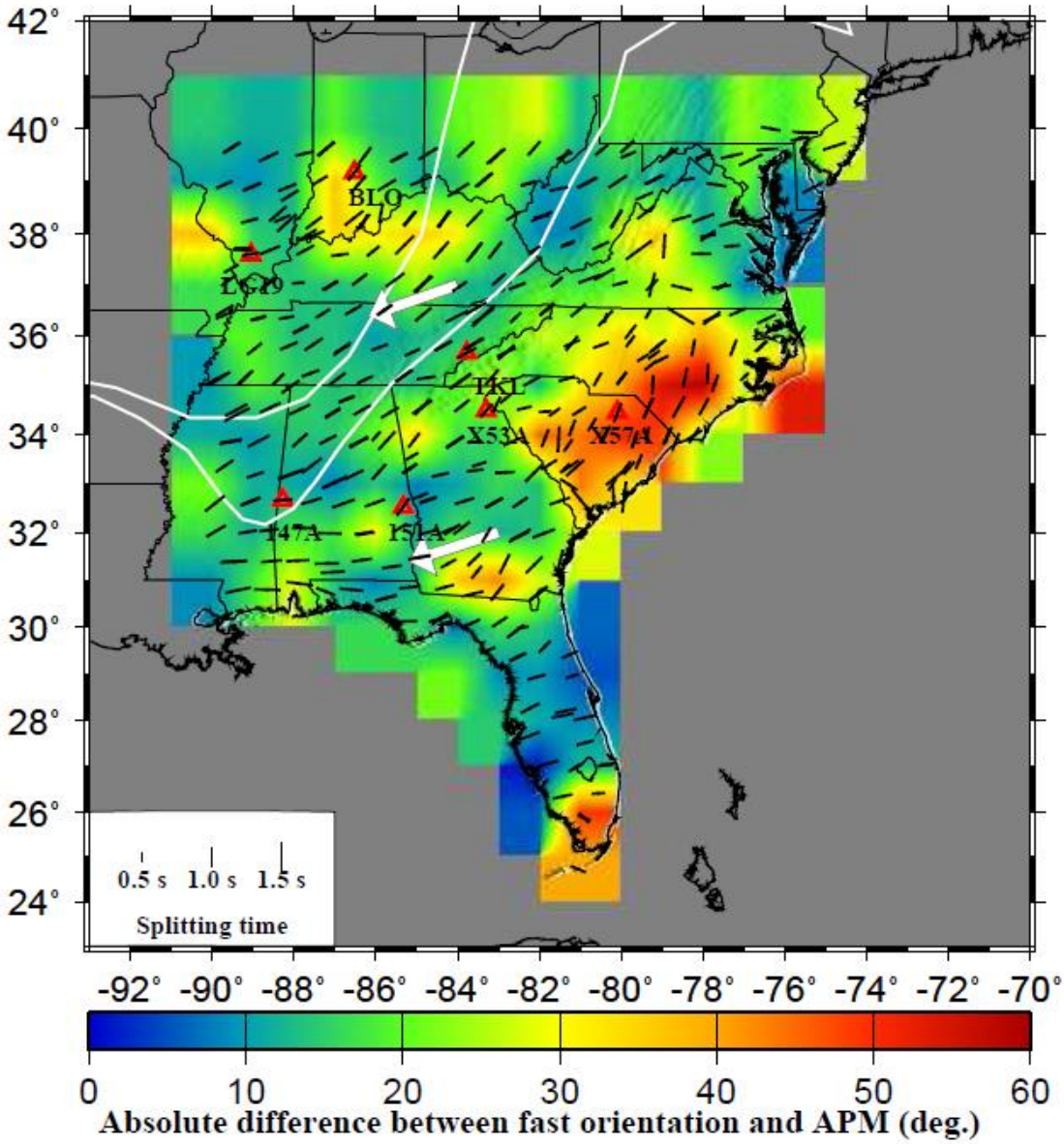

Figure 3.2. Station-averaged SWS measurements plotted on map of absolute difference between the observed fast orientations and the APM direction (white arrows). The white solid lines are major tectonic boundaries. The orientation of the black bars represents the fast polarization orientation, and the length is proportional to the splitting time. The red triangles are the stations with possibility to have systematic azimuthal variations of the splitting parameters.

generally consistent with the APM direction with a few exceptions in the New Madrid seismic zone, north part of Kentucky and south of Indiana. These exceptions have a difference of 30°-40° with the APM direction. The fast orientations in the Greenville province spatially correlate with the APM direction. The two large and continued deviations are observed in the Appalachian province. One apparent deviation is located in the Appalachian mountain belts along the boundary of the Greenville and Appalachian provinces. The absolute difference is about 20° which corresponds to the strike of the orogeny. The other significant difference is found in North Carolina and South Carolina in which the fast orientations are mostly N-S which is 50°-60° away from the APM. Along the edge of the north part of the continent, the averaged fast orientations are mainly E-W, which has a 20°-30° difference with the APM direction. For the rest part of the area in the Appalachian province, the absolute difference is less than 10°.

3.4 SPATIAL DISTRIBUTION OF SPLITTING TIMES

The spatial distribution of splitting times is shown in Figure 3.3. This distribution is measured by the averaged value of individual splitting times at the piercing points of 200 km deep in overlapping 1° by 1°blocks with a moving step of 0.01°, and by resampling to a resolution of 0.1° for display. The general distribution of the splitting times is decreasing from northwest to southeast. The average δt value of entire study area is about 1.0 s, which is consistent with the globally averaged value [Silver, 1996]. The largest splitting times are found in the southwestern and northeastern Appalachian province, which are larger than 1.1 s. The continental interior is characterized by

relatively small splitting times between 0.6 s to 0.8 s with some exceptions located in the vicinity of the Appalachian mountain belts and the northern part of the Yavapai province.

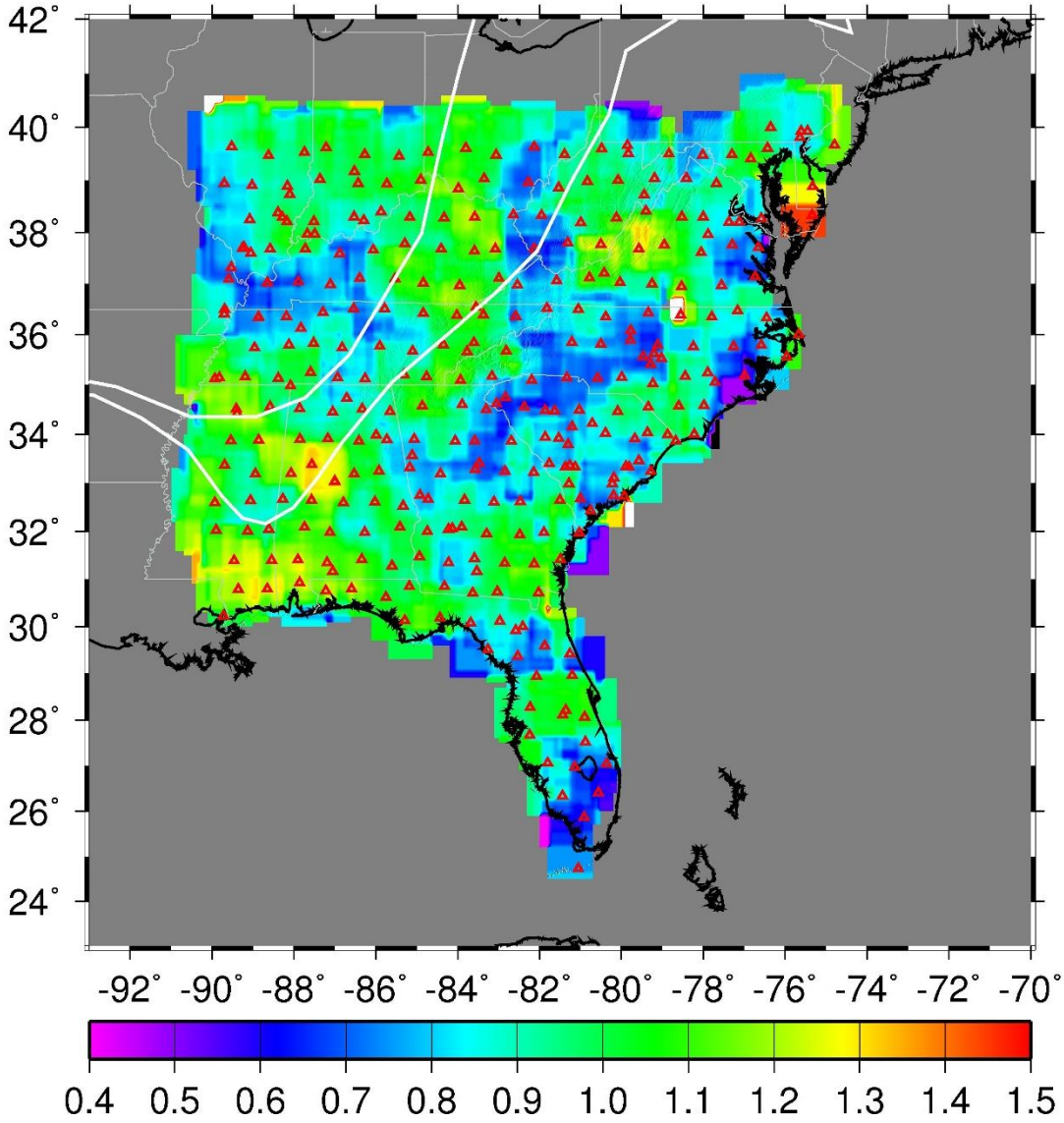

Figure 3.3 Spatial distribution of splitting times. Red triangles are seismic stations used in the study. Solid white lines denote the boundaries of tectonic provinces.

4. DISCUSSION

4.1 COMPARISON WITH PREVIOUS STUDIES

In general, the measurements from this study are consistent with those from other studies at stations located in the Appalachian mountain belts which proposed strike-parallel fast orientations. In the surrounding regions such as the Greenville province, the NE-SW fast orientations are consistent with those from other studies as well [Long et al., 2010; Wagner et al., 2012]. Due to the complex tectonic processes of the eastern North America plate, the interpretation of the observed fast orientations is complicated along the coastal area. There are some discrepancies in the eastern coastal area between this study and the studies by Long et.al. [2010], Wagner et al. [2012], and Long et al. [2015]. They reported a large quality of null measurements in the eastern coastal area. The stations (KMSC, WOAK, DWDAN, AGBLF, BLACK, TIMBR, NHSC, BTRCK, GOGA, FA05 and FA06) are proposed as only-null-measurements in Wagner et al. [2012]. Undeniably, some null measurements are found in some stations, but some Quality A and Quality B measurements are also found at each station (see Figures 4.1-4.8 for examples) near the coastal area.

Barruol et al. [1997b] also proposed the absence of detectable splitting which is attributed to igneous intrusions in the eastern Appalachians. As Wagner et al. [2012] mentioned in their paper, the discrepancies of SWS measurements among the different studies in the coastal region may result from different processing procedures, frequency content, and measurement methods.

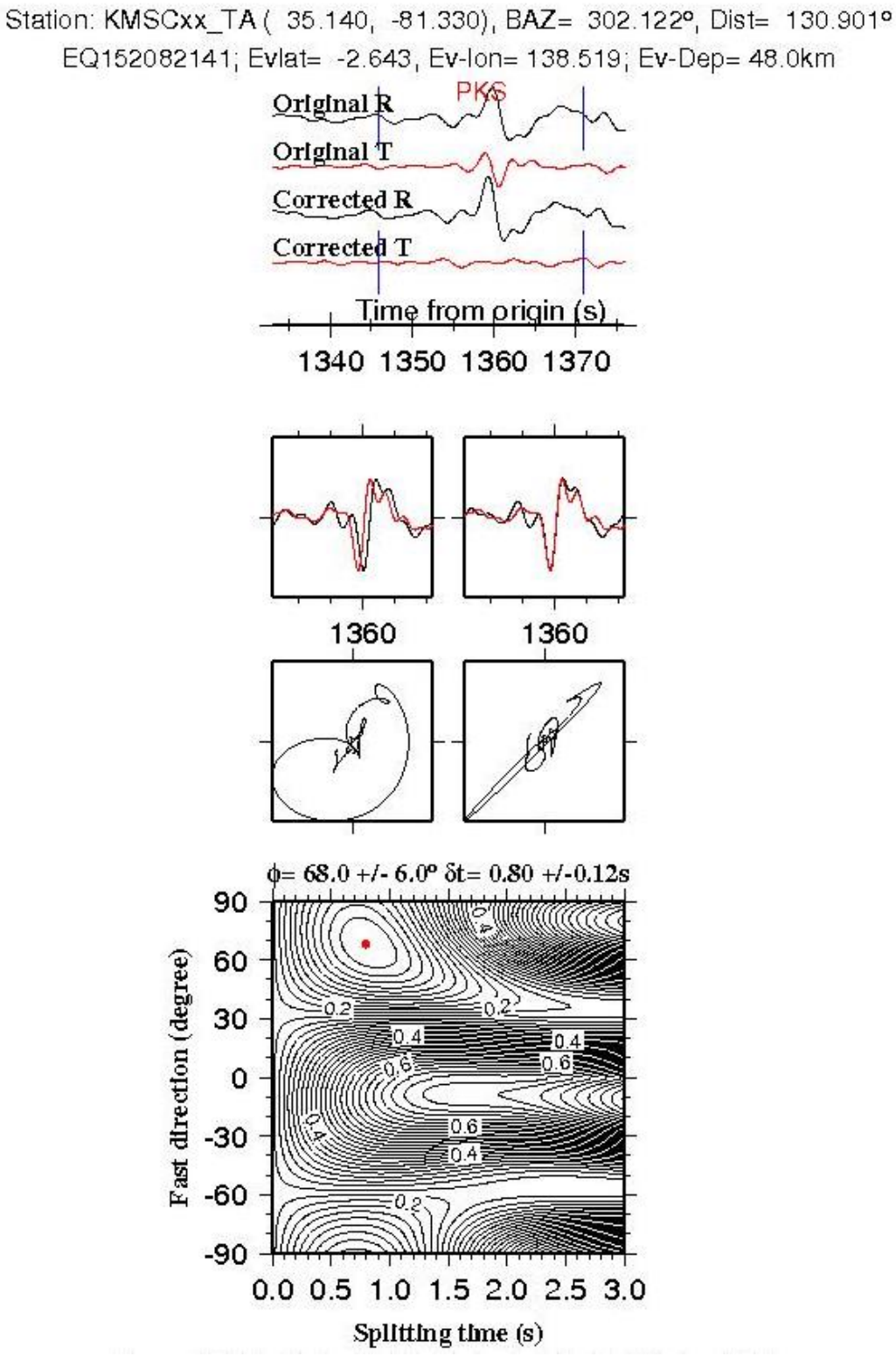

Figure 4.1 Quality A examples of station KMSC.

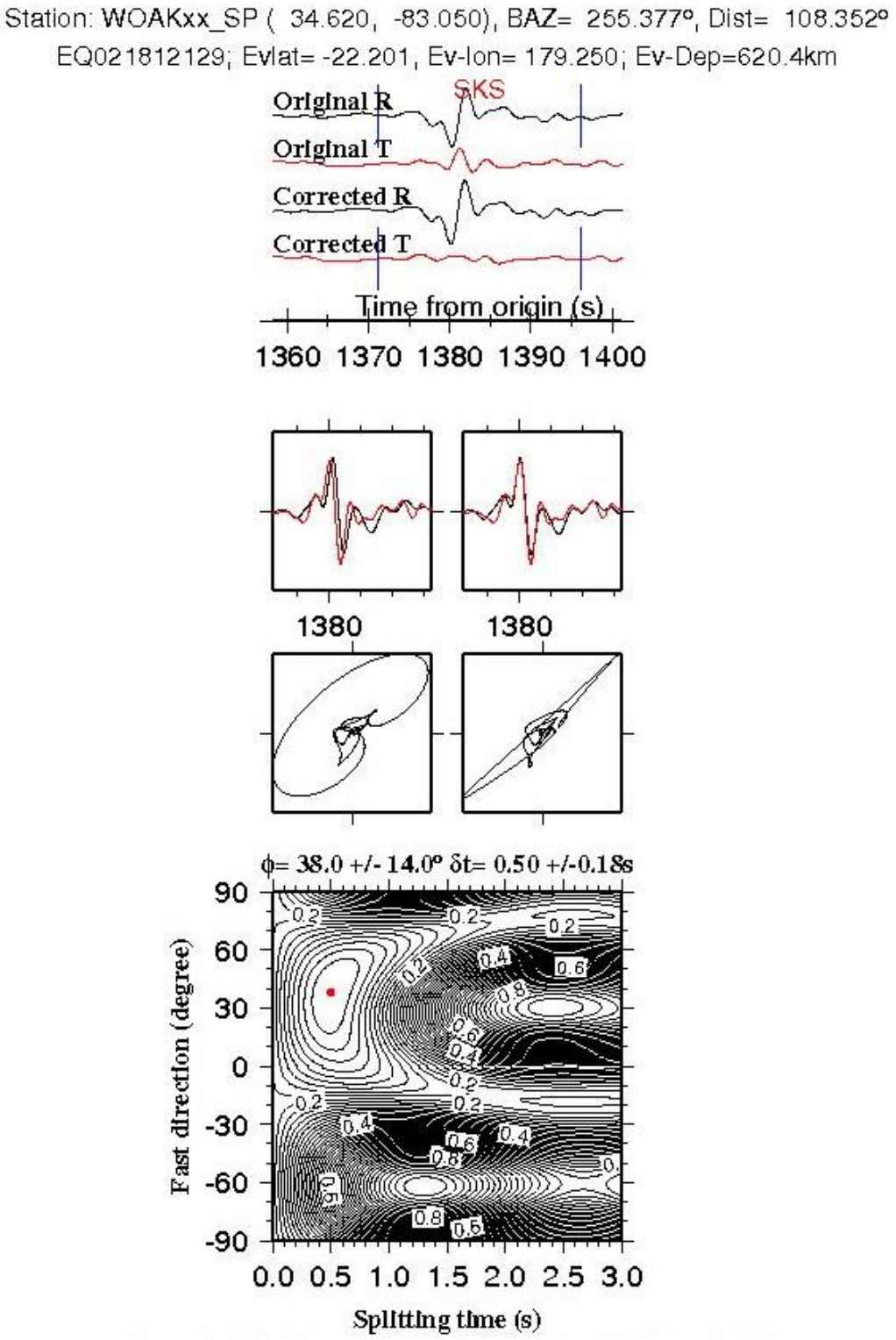

Figure 4.2 Quality A examples of station WOAK.

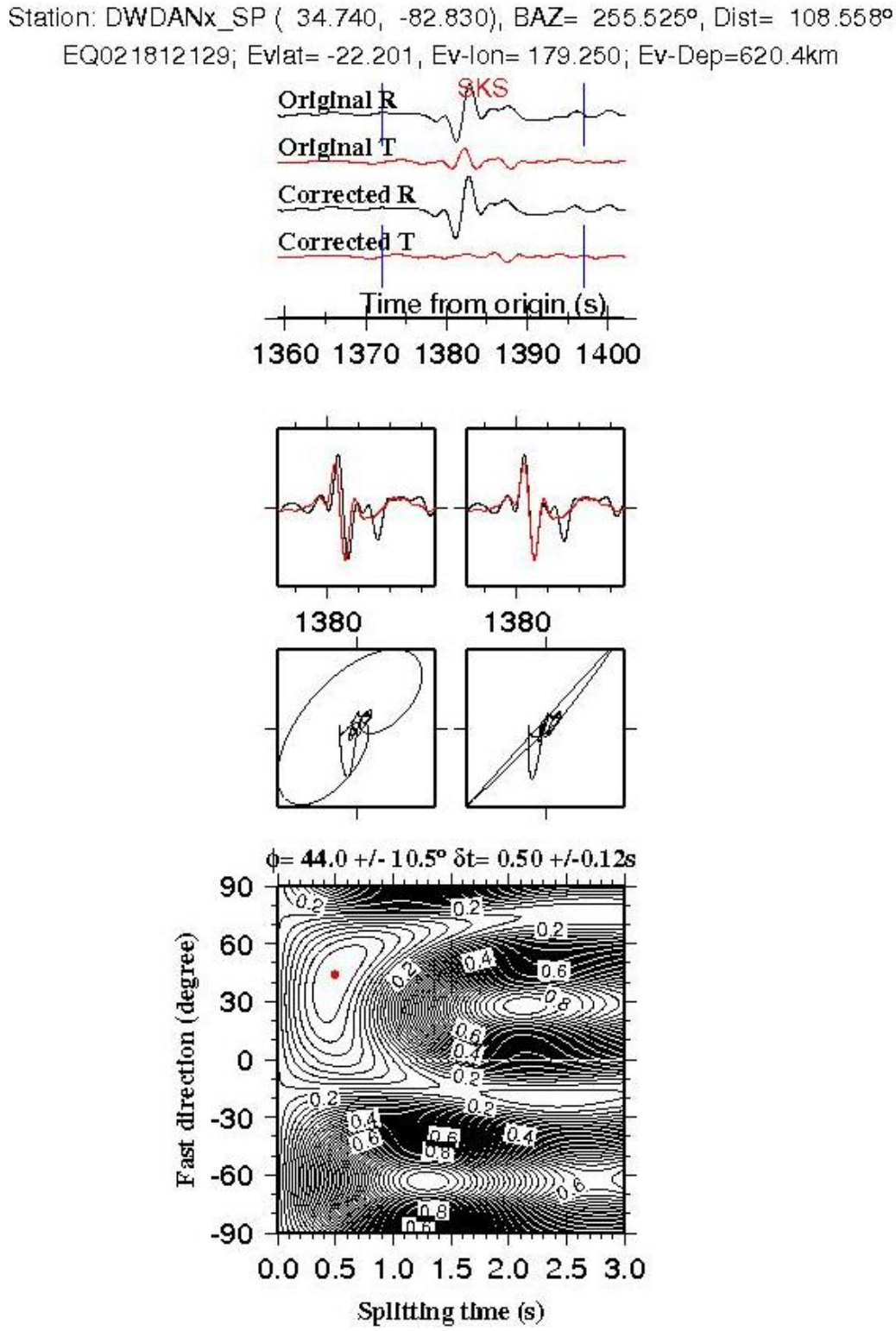

Figure 4.3 Quality A examples of station DWDAN.

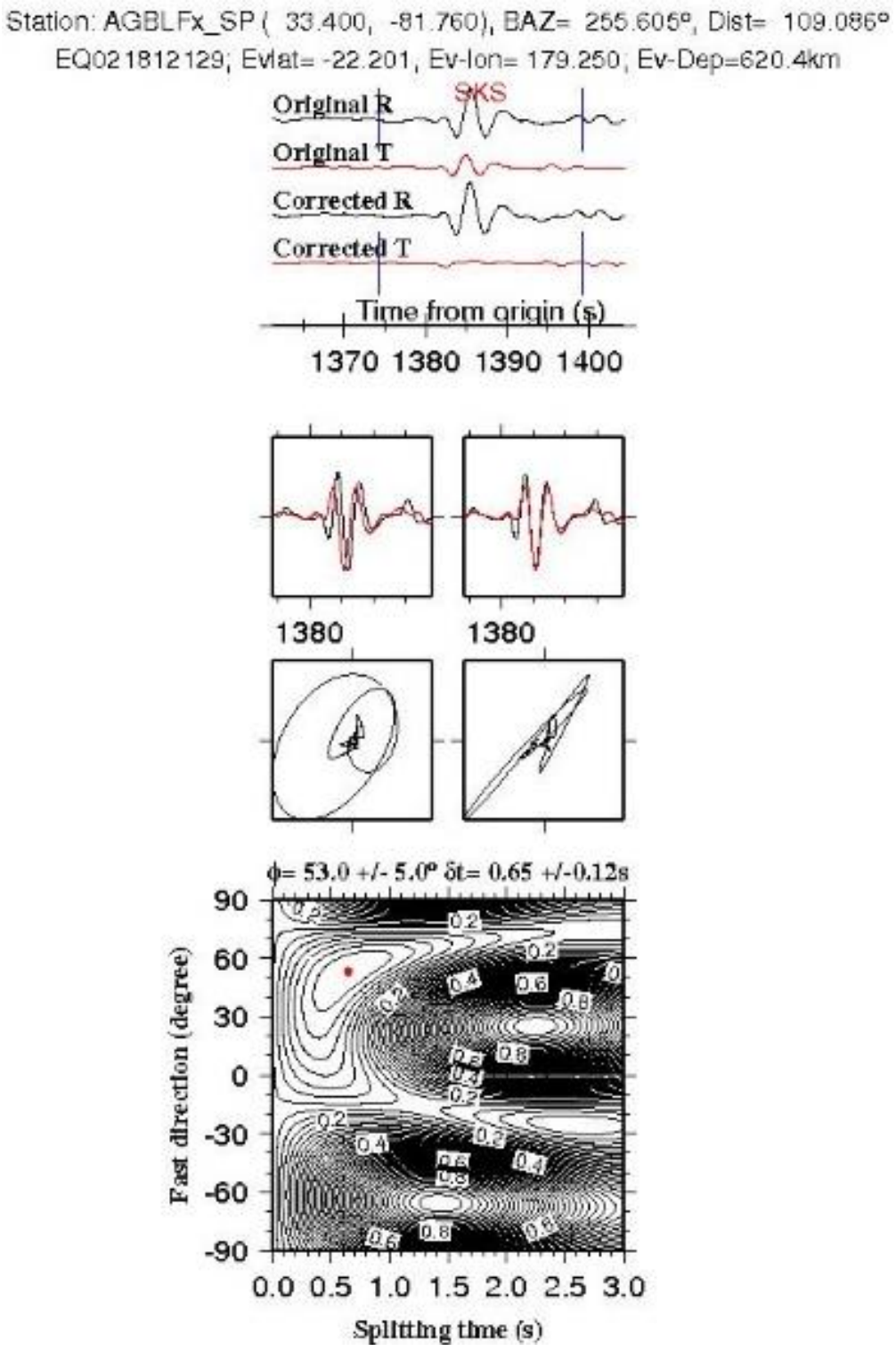

Figure 4.4 Quality A examples of station AGBLF.

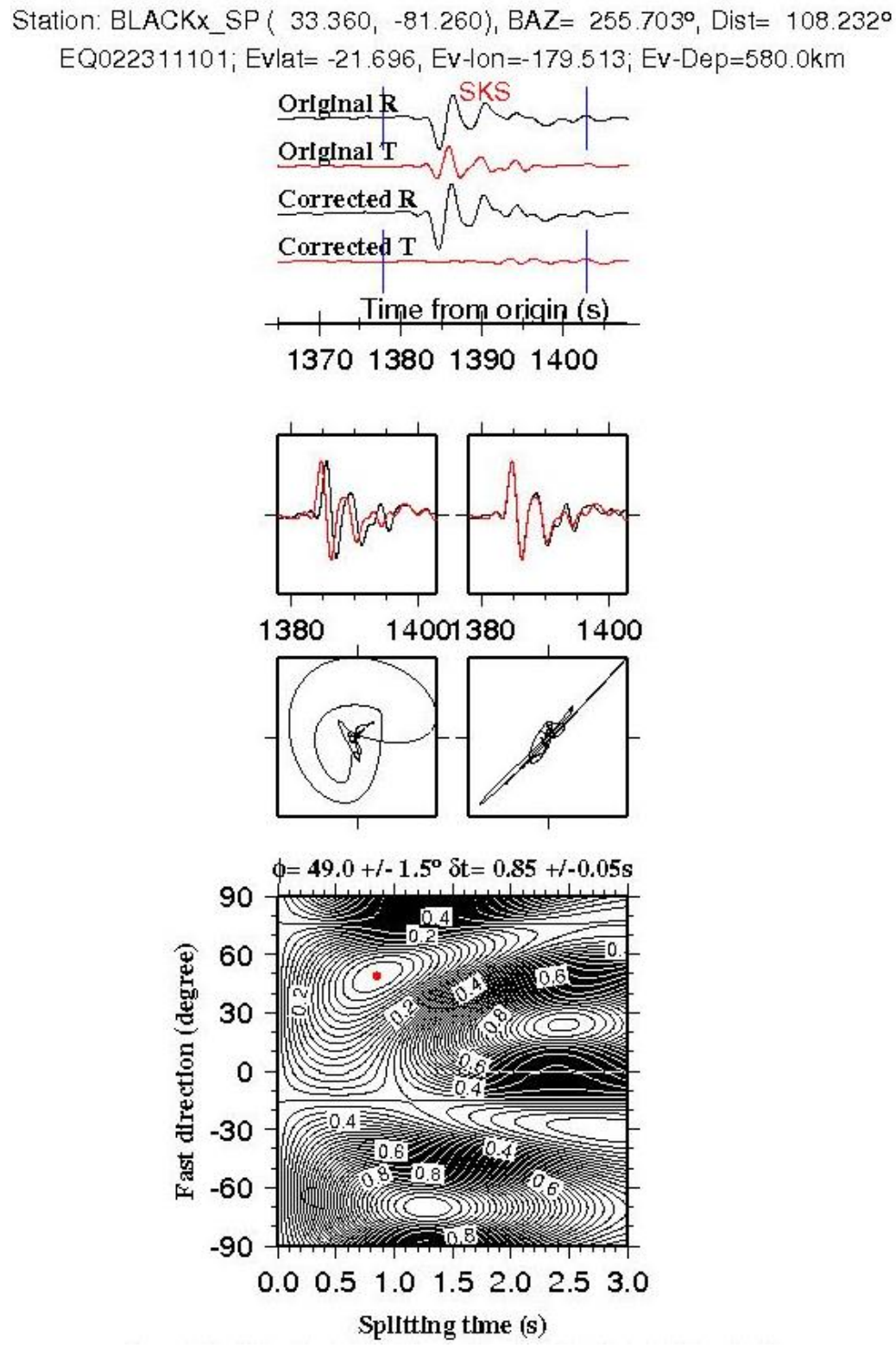

Figure 4.5 Quality A examples of station BLACK.

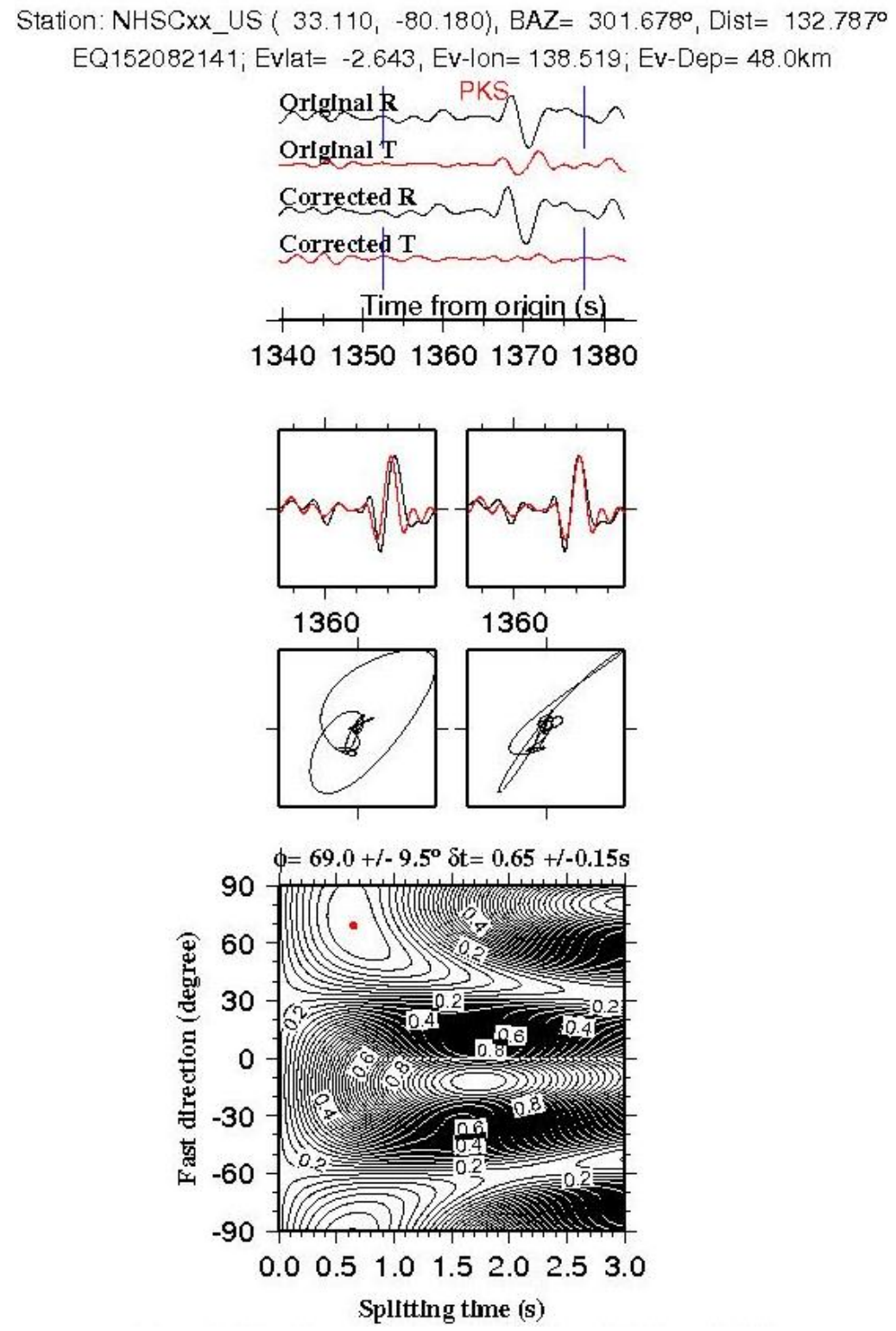

Figure 4.6 Quality A examples of station NHSC.

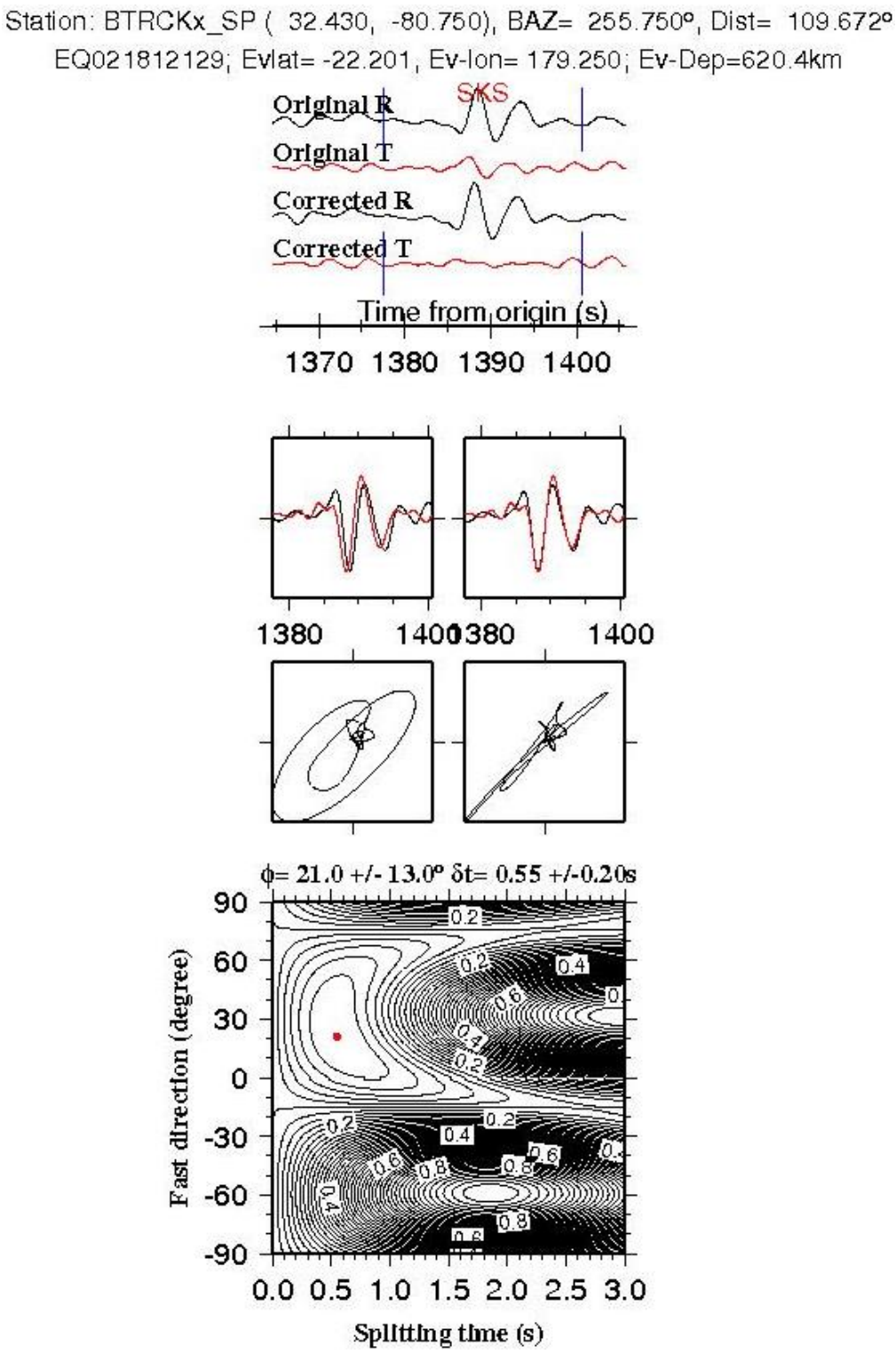

Figure 4.7 Quality A examples of station BTRCK.

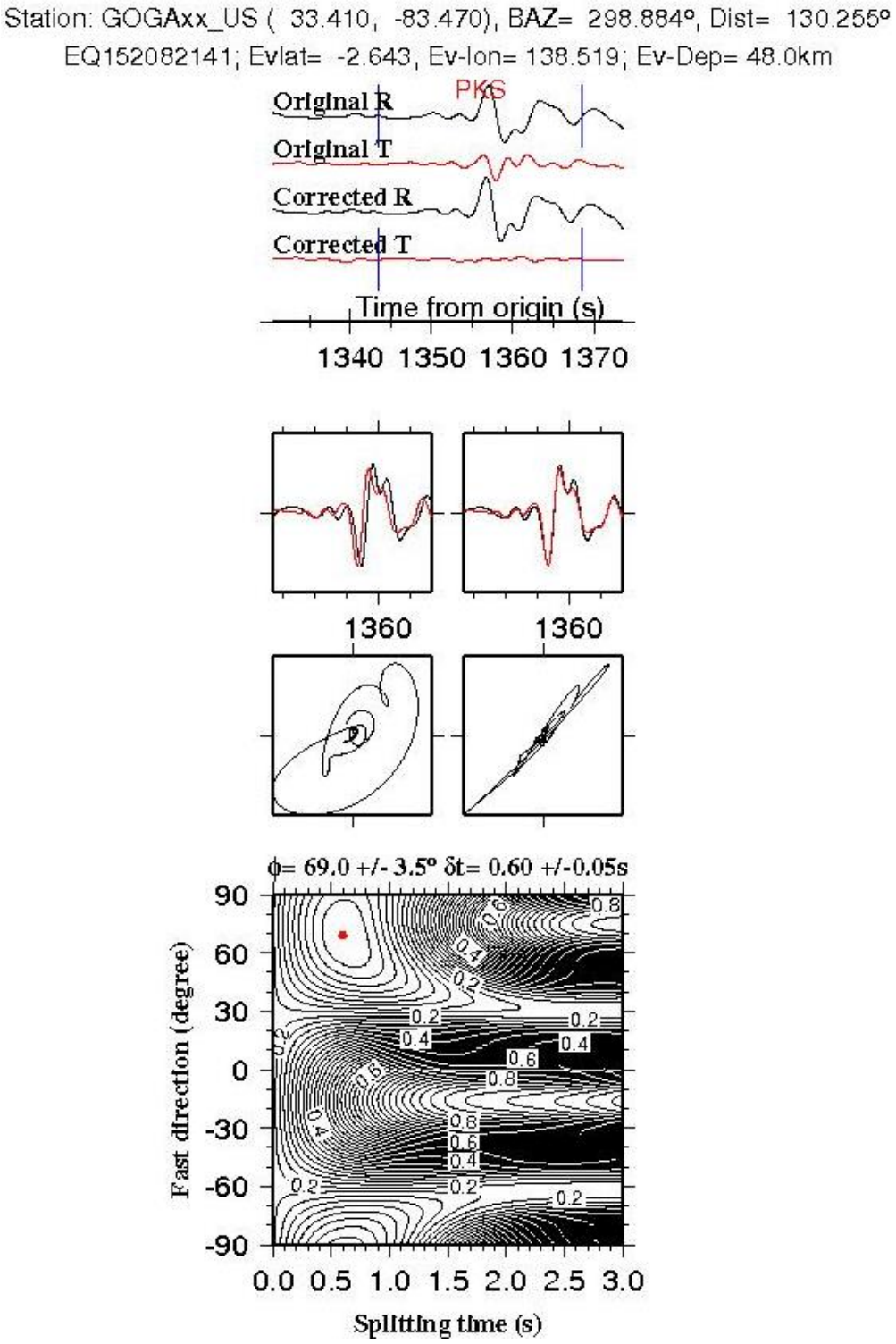

Figure 4.8 Quality A examples of station GOGA.

4.2 THE ARGUMENT OF COMPLEX ANISOTROPY

Azimuthal variations of splitting parameters with a π /2 periodicity in apparent splitting parameters are a diagnostic of double-layer anisotropy with a horizontal axis of symmetry [Silver and Savage, 1994]. Most of the stations do not have sufficient back azimuthal coverage to test this prediction, but the analysis of Long et al. [2010] ruled out the existence of complex anisotropy for many of the permanent stations (e.g., NHSC, CNNC, CBN, BLA, MCWV, TZTN, LRAL). In this study with no-null measurements, the observed splitting measurements of all the 382 stations are visually examined to identify the ones with systematic azimuthal variations. After visually checking the azimuthal variations of the fast orientations, only seven stations have the possibility to be stations with 2-layer anisotropy. However, splitting parameters lack sufficient azimuthal coverage at these seven stations, preventing a formal grid-search. Figures 4.9-4.11 show the examples of measurements from those stations. Note that attempts have been made to use data from nearby stations to search for the 2-layer parameters. Unfortunately, these nearby stations have demonstrated clear simple anisotropy. In addition, the averaged fast orientation of each of the seven stations is near parallel to the surrounding stations (see stations in Figure 3.2).

Comparing to the stations located in the continental interior, stations have different fast orientation patterns near the coastal area. These stations do not have decent azimuthal variations to test the existence of multiple-layered anisotropy. Using the individual stations or groups of nearby stations to search for the 2-layer parameters near the coastal area, we barely observe the azimuthal variations of splitting parameters with a π /2 periodicity in most of the stations.

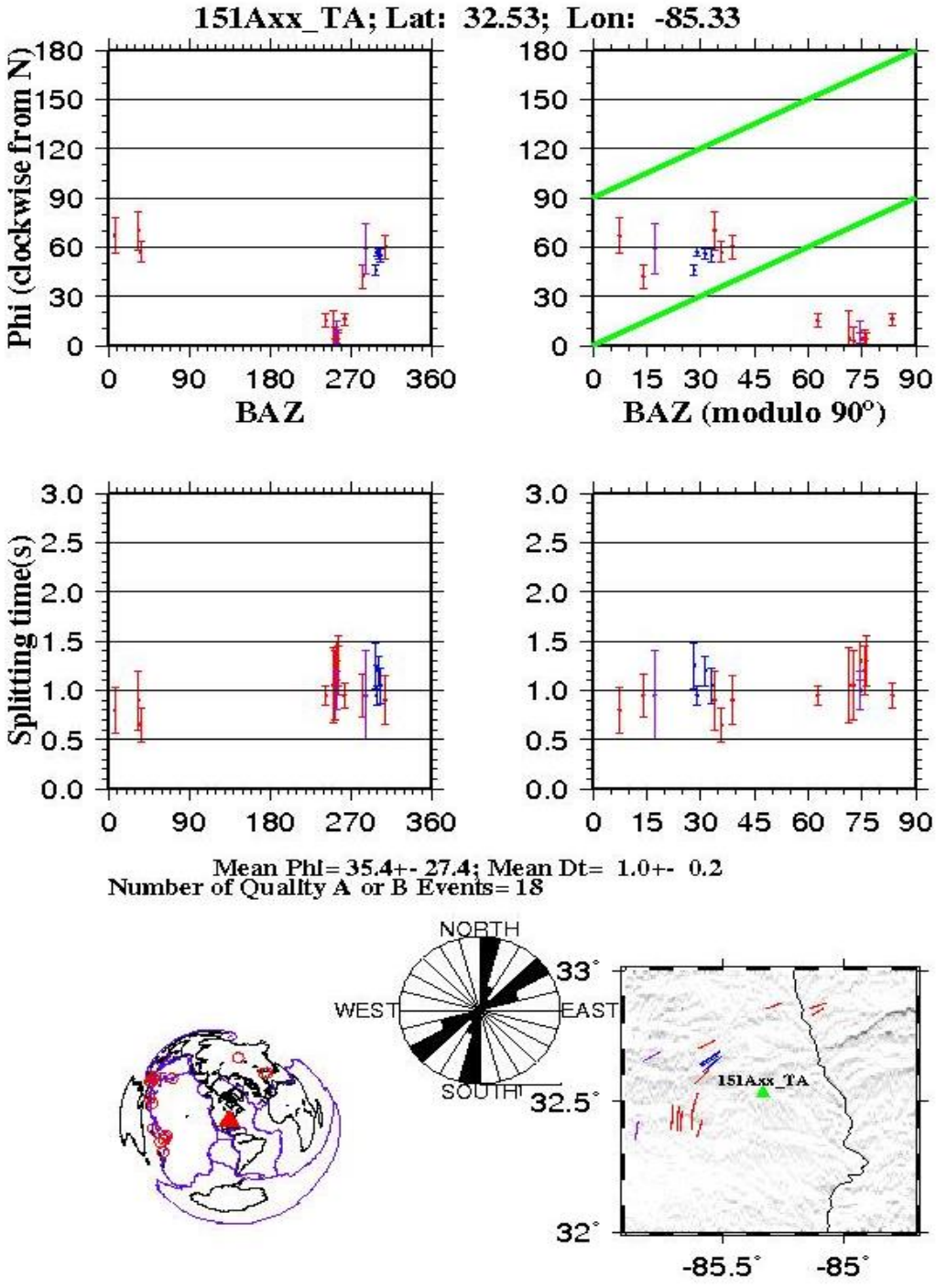

Figure 4.9 Azimuthal variations of fast orientations (top) and the splitting times (middle) and the distribution of the events and rose diagram of measurements (bottom) for station 151A demonstrate the presence of two-layer anisotropy.

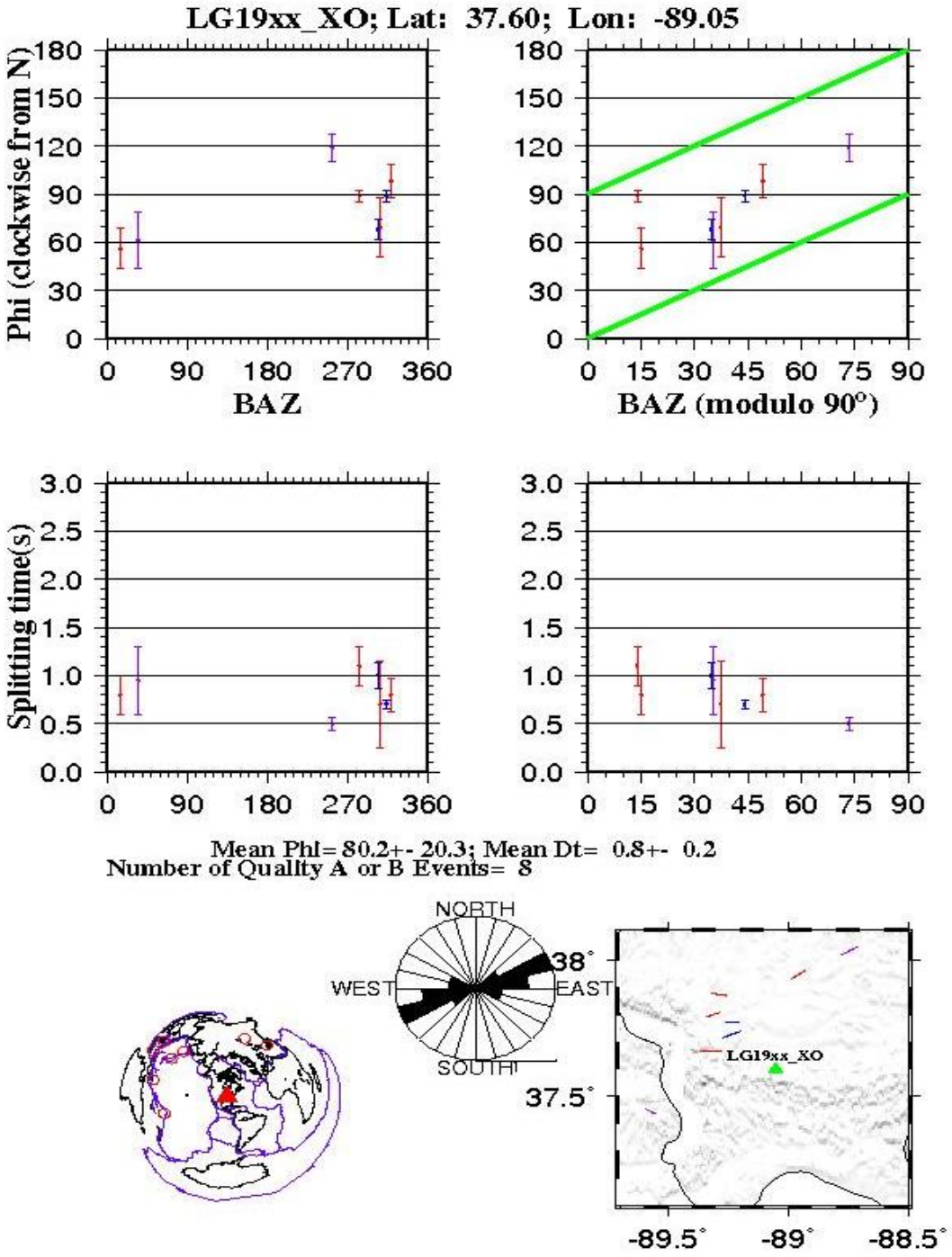

Figure 4.10 Azimuthal variations of fast orientation (top) and the splitting times (middle) and the distribution of the events and rose diagram of measurements (bottom) for station LG19 demonstrate the presence of two-layer anisotropy.

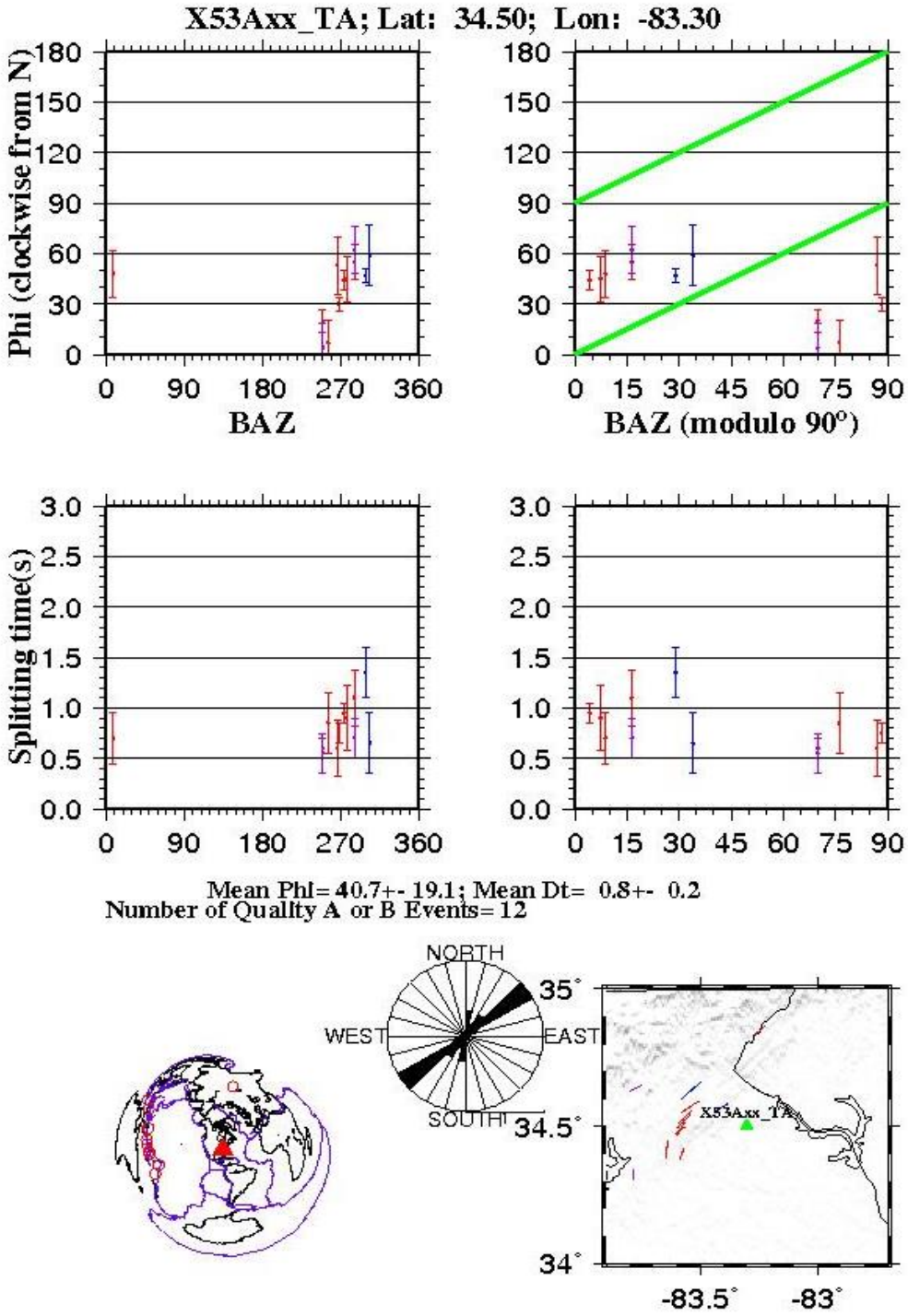

Figure 4.11 Azimuthal variations of fast orientation (top) and the splitting times (middle) and the distribution of the events and rose diagram of measurements (bottom) for station X53A demonstrate the presence of two-layer anisotropy.

Figures 4.9-4.11 display the distribution of the azimuthal variations of δt and ϕ, also with rose diagram of ϕ.

Near the coastal area, some stations have a relatively small amount of Quality A and Quality B measurements. However, these stations have been suggested as null-measurement stations [Long et al., 2010; Wagner et al., 2012; and Long et al., 2015]. It is possible that the top layer has a fast orientation that is perfectly orthogonal to the APM direction. This prediction was ruled out by Long et al. [2010] and also can be ruled out by our study. According to our study, we do not find any two-layer anisotropy in this region. Furthermore, we proposed that stations are mostly non-null instead of null in the debatable area.

4.3. ESTIMATION OF ANISOTROPY DEPTH BENEATH THE STUDY AREA

Once we concluded the pervasiveness of simple layer of anisotropy, we next estimate the depth of this anisotropy. This estimation can provide robust evidence that the observed seismic anisotropy using SWS is from the lithosphere, asthenosphere or a combination of the two [Long and Silver, 2009; Savage, 1999]. If the fast polarization orientation is in alignment with the APM direction, the splitting parameters will primarily reflect the asthenosphere source [Conrad et al., 2007]. The plate motion will align the mineral such as olivine to the same orientation which is the infinite strain axes. Therefore, the fast polarization orientations will be parallel to either the absolute plate motion shear or the mantle flow direction [Karato et al., 2008; Huang et al., 2011].

On the contrary, if the anisotropy reflects the lithospheric origin, the SWS observation would be expected to be parallel to the surface geological features such as mountain belts, major faults, and extensional rifts including continental margins [Nicolas and Christensen, 1987; Nicolas, 1993; Savage, 1999; Silver, 1996; Gao et al., 1997].

In this study we use the spatial variation factor approach, which was proposed by Gao et al. [2010] and Liu and Gao [2011] to estimate the depth of anisotropy. The estimation theory, method, and a detailed FORTRAN program are published in Gao and Liu [2012]. We divided the area into three geological provinces and processed the measurements located in these three provinces separately. The resulting depths of the Yavapai (Figure 4.12) and the Greenville provinces (Figure 4.12) are around 220 km. In the result of Yuan et al. [2014] (Figure 4.13) for the depths of the 250 km and 300 km, the 0% to 2% dlnVs indicates the normal to moderate high-velocity structure locate at this area. The results are consistent with the 220 km depth estimated from this study. In area A of the Appalachian province, the estimated anisotropy depth is 240 km (Figure 4.12), which corresponds to 0% dlnVs at 250 km. Notably, area B has an anisotropy depth of 165 km (Figure 4.12), with relatively small splitting times. Also, the dlnVs values abrupt change from ~2% to ~0% at the 200 km depth comparing to 165 km in area B. In area B and area C, the estimated anisotropy depth is about 165 km (Figure 4.12). This value is reasonable for thin continental margin. The dlnVs value is 2% at 300 km in this area from the study of Yuan et al. [2014] (Figure 4.13). It remains a high-velocity structure at 150 km. So the relative small value of the anisotropy depth in area C is reasonable and correlates to the tomography study.

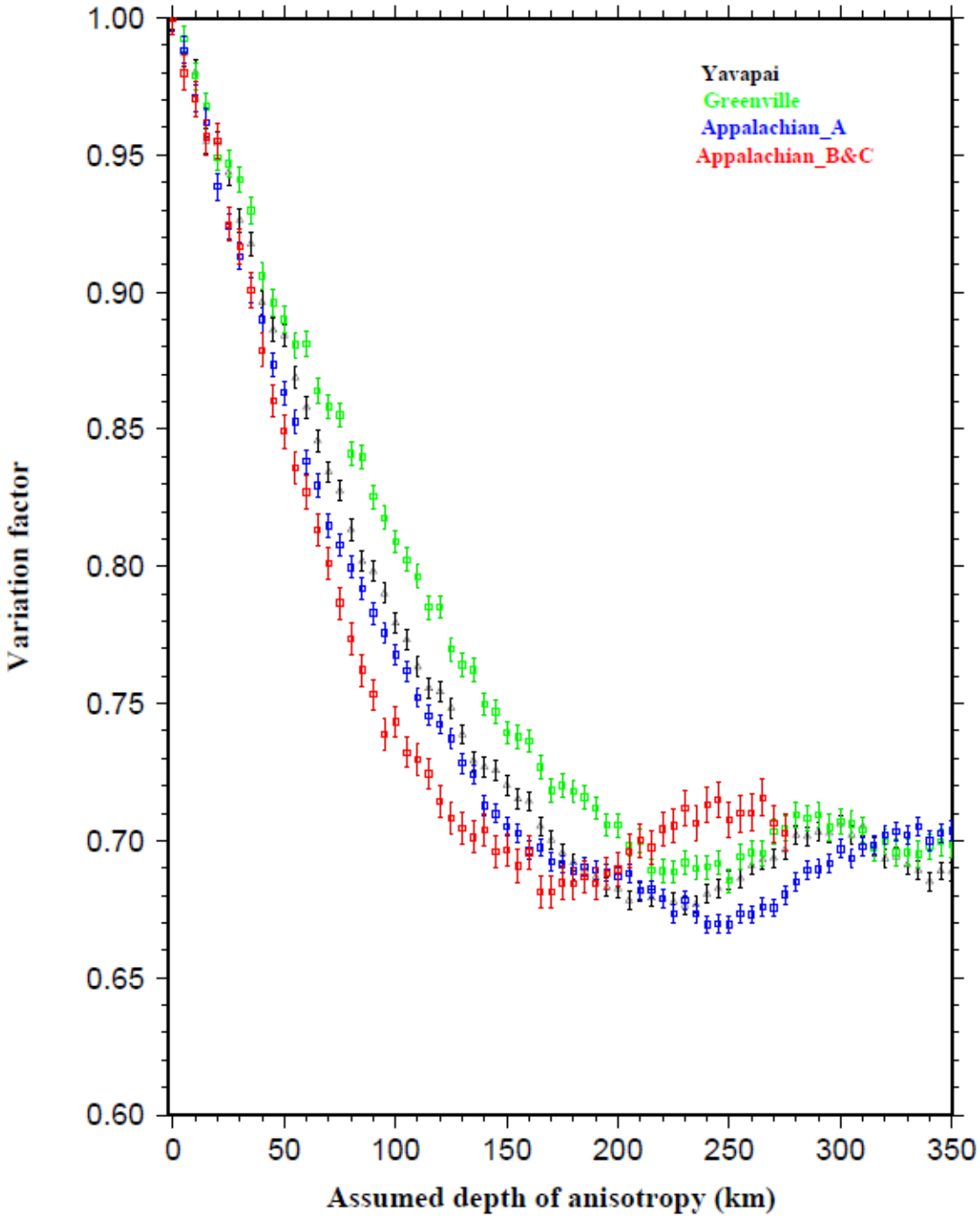

Figure 4.12 Spatial variation factors as a function of assumed depth of the source of anisotropy for the different provinces.

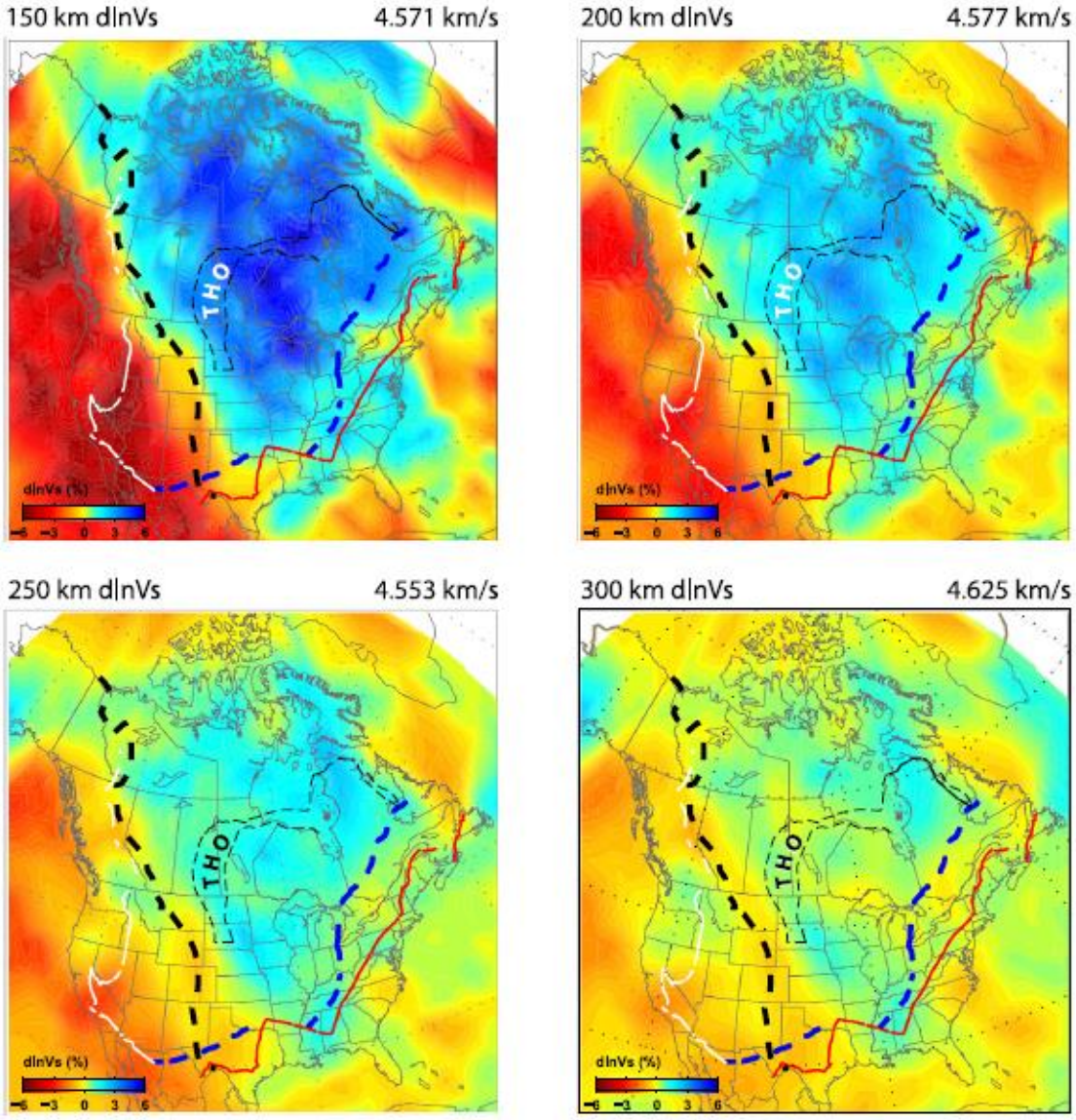

Figure 4.13 3D isotropic shear wave velocity structure of the North American continent. Map views are shown from150 km down to300 km [Yuan et al., 2014].

4.4 CONTRIBUTIONS TO OBSERVED ANISOTROPY: PRELIMINARY MODEL

In the vicinity of the Appalachian mountain belts, the fast orientation is perpendicular to the shortening direction which is parallel to the strike of the mountain belts. Also, the relative small splitting time, 0.6 s-0.7 s (Figure3.3), are found in this area.

The compressional event between North American Plate and Eurasian Plate that formed the Appalachian mountain might have affected the fabric's reorganization. The subduction and igneous intrusion happened before the compressional event and contributed to the first rising of Appalachian Mountain might also affect the anisotropy. The observed SWS measurement and lithospheric anisotropy result are consistent with the previous studies.

For the rest of area, it lacks significant evidence to support the lithospheric contribution to the observed anisotropy. Different geodynamic modeling and seismic tomography studies [Becker et al., 2008; Forte et al., 2007] suggested a dominantly northeastward-directed asthenospheric flow probably induced by the sinking of the Farallon plate in the lower mantle beneath the New Madrid seismic zone. Beneath the cratonic root, the relative movement and partial coupling between the lithosphere and asthenosphere can also lead to simple flow in the upper asthenosphere [Yang et al., 2014; Refayee et al., 2014]. Both of the mentioned flow systems may contribute to the observed APM-parallel anisotropy.

This study proposes that beneath the southeastern U.S., the southwestward moving North America craton root deflects asthenospheric flow along its edge (Figure 4.14). The flow moves from W turns to NNE at the southeast corner of the craton root. This eastward edge-parallel flow is consistent with the model proposed by Refayee et al. [2014] (Figure 4.15). In the southeastern costal area, the flow is nearly parallel to the edge of the southeastern continental craton. Based on the depth estimates and the SWS measurements, most of the observed anisotropy has an origin in the upper asthenosphere. In the Yavapai and Greenville provinces, the spatial consistency between the observed

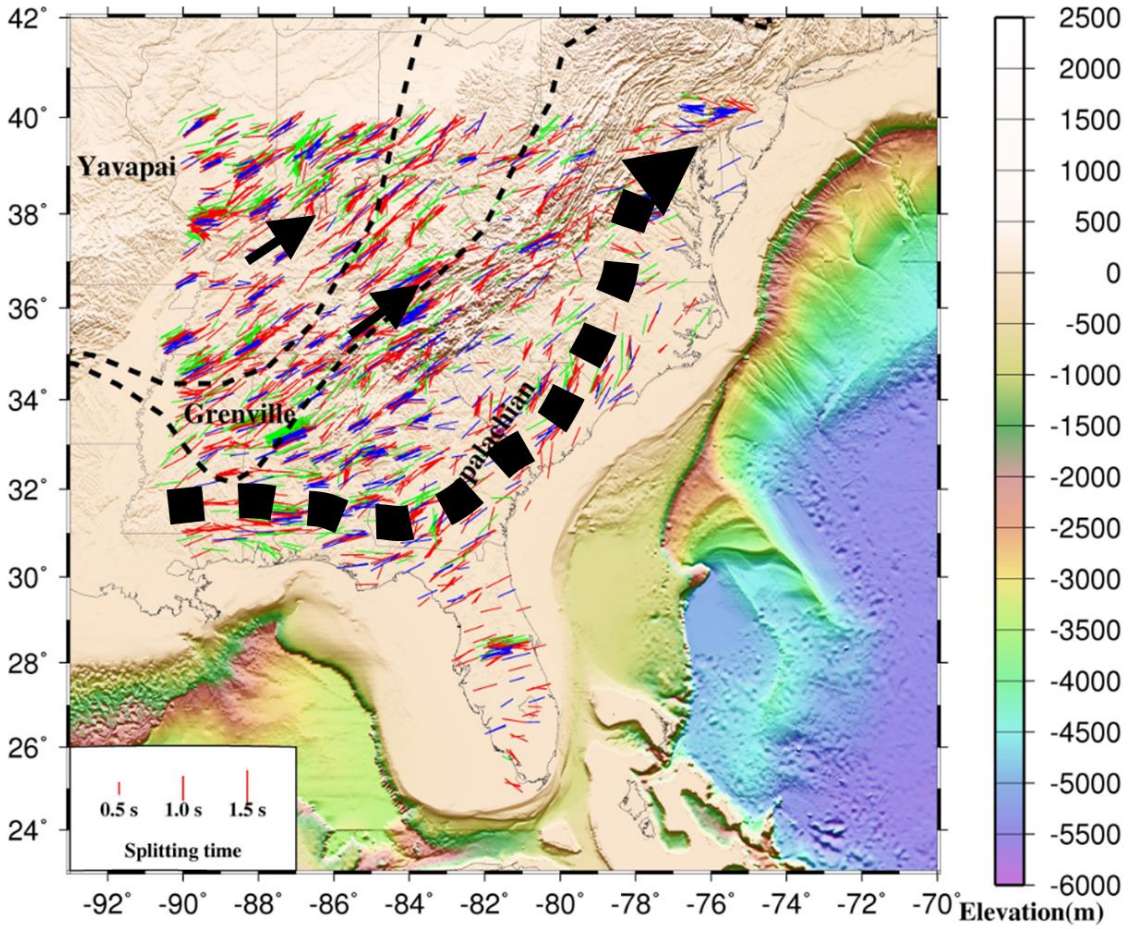

Figure 4.14 Schematic diagram showing direction of flow lines in the asthenosphere. The thick dash line represents flow deflected by the root of the North American craton. The black arrows indicate the APM-parallel direction flow system.

fast orientations and the APM direction indicates significant contribution of asthenospheric flow. Such APM-parallel anisotropy in the upper asthenosphere is indicative of a certain degree of lithosphere–asthenosphere coupling [Marone and Romanowicz, 2007]. The horizontal flow beneath the North American continental interior (Figure 4.14) is consist with global flow proposed by Becker et al. [2008]. However, the deflected asthenospheric flow found along the southeastern continental edge is not proposed in the study of Becker et al. [2008].

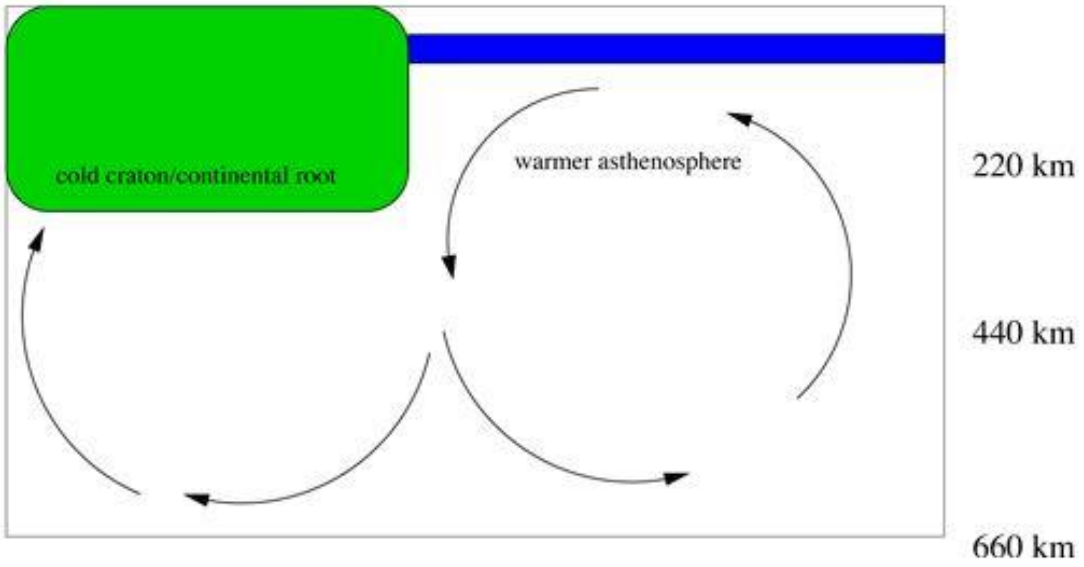

Figure 4.15 Schematic diagram showing direction of flow lines in the asthenosphere in the southwestern edge of the North American craton [Refayee et al., 2014].

In the vicinity of the eastern Appalachian province, the distribution of Quality A and Quality B measurements is more sparse than other area. This intriguing difference has been explaining by several studies. The null measurements have been proposed by Long et al. [2010] and Long et al. [2015] at the eastern coastal area. There are two possible reasons for the observed null measurements. First, the anisotropic directions of the two layers may be perpendicular to each other, so that the observed splitting can be perfectly canceled. Thus, we cannot observe the splitting. This factor can be ruled out since complex anisotropy is not observed in this area. Although the splitting data (Quality A and Quality B measurements) are limited to the coastal area, we still observed splitting measurements at each station instead of null measurements. Second, small-scale vertical flow may cause the sparse splitting observation (Figure 4.16). Edge-driven-convection may occur at the boundary between the thick North American craton and thinner coastal

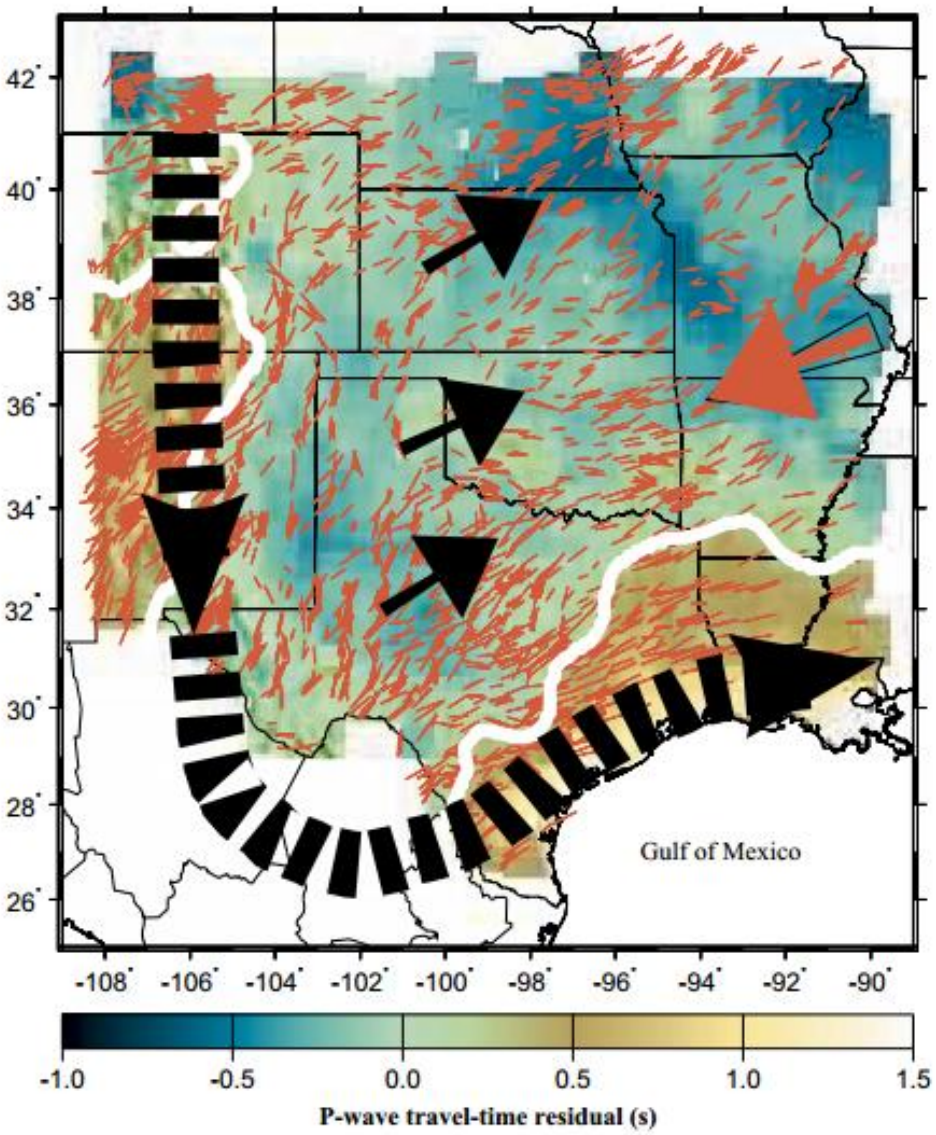

Figure 4.16 Schematic of small-scale convective flow along a craton boundary. The green rectangular represents the craton root, blue rectangular represents thin lithosphere. The arrows illustrate the resulting flow pattern [King and Anderson, 1998].

lithosphere [King and Anderson, 1998; King and Ritsema, 2000]. Edge-driven-convection instability is driven by the temperature discontinuity at the vertical wall separating the cold and stable craton from the warmer asthenosphere, aligning the olivine a-axis vertically and leading to weak anisotropy.

The other mechanism leading to vertical flow has been proposed by Van der Lee et al. [2008], who suggested the upwards transport of volatiles from the deep Farallon slab in the mid-mantle as an explanation for a persistent low-velocity anomaly present beneath the east coast of the US in surface wave tomography models. The vertical upwards flow implied by such a model might cause asthenospheric anisotropy with a vertical axis of symmetry beneath the region.

5. CONCLUSIONS

Systematic spatial variations of shear-wave splitting parameters are observed beneath the southeastern North American continent and adjacent areas. Lack of azimuthal variations suggests dominantly single layer of anisotropy. Spatial coherency analysis of the splitting parameters suggests that the observed anisotropy is mostly from the upper asthenosphere, implying a certain degree of coupling between the lithosphere and the asthenosphere.

The spatial consistency between the observed fast orientations and the absolute plate motion direction of the North American plate and depth distribution of the source of anisotropy suggest a significant asthenospheric contribution to the observed XKS splitting. The deflection of asthenospheric flow around the edges of the craton is responsible for the edge-parallel fast orientations observed along the southern and eastern margins of the study area.

Except for the Appalachian orogenic belt in which the fast orientations are parallel to the strike of the mountain belts, the fast orientations are in acceptable agreement with the orientation of flow direction, suggesting an insignificant contribution from the lithosphere.

6. BIBLIOGRAPHY

Anderson, D. L. (1989), Theory of the Earth. Blackwell Scientific Publications. Boston. Ando, M. 1984. ScS polarization anisotropy around Pacific Ocean, J. Phys. Earth 32, 179–195.

Barruol, G., P. G. Silver, and A. Vauchez (1997b), Seismic anisotropy in the eastern United States: Deep structure of complex continental plate, J. Geophys. Res., 102, 8329-8348.

Becker, T. W. (2008), Azimuthal seismic anisotropy constrains net rotation of the lithosphere, Geophys. Res. Lett., 35, L05303, doi:10.1029/2007GL032928.

Cawood, P. A., and C. Buchan (2007), linking accretionary orogenesis with supercontinent assembly, Earth Sci. Rev., 82, 217–256, doi: 10.1016/j.earscirev.2007.03.003.

Conrad, C. P., M. D. Behan, and P. G. Silver (2007), Global mantle flow and the development of seismic anisotropy: differences between the oceanic and the continental upper mantle, J. Geophys. Res., 112, B07317. DOI: 101029/2006JB004608.

Fouch, M.J., and S. Rondenay (2006), Seismic anisotropy beneath stable continental interiors, Phys. Earth Planet. Int., 158, 292-320.

Forte, A. M., J. X. Mitrovica, R. Moucha, N. A. Simmons, and S. P. Grand (2007), Descent of the ancient Farallon slab drives localized mantle flow below the New Madrid seismic zone, Geophys. Res. Lett. 34, L04308.

Fouch, M. J., K. M. Ficher, E. M. Parmentier, M. E. Wysession, and T. J. Clarke (2000), Shear wave splitting, continental keels, and patterns of mantle flow, J. Geophys. Res., 105, 6255-6275.

Gao, S., P. M. Davis, H. Liu, P. D. Slack, A. W. Rigor, Y. A. Zorin, V. V. Mordvinova, V. M. Kozhevnikov, and N. A. Logatchev (1997), SKS splitting beneath continental rift zones, J. Geophys. Res., 102, 22-781.

Gao, S. S., and K. H. Liu (2009), Significant seismic anisotropy beneath the southern Lhasa Terrane, Tibetan Plateau, Geochem. Geophys. Geosyst., 10, 597 Q02008, DOI:10.1029/2008GC002227.

Gao, S. S., and K. H. Liu (2012), AnisDep: A FORTRAN program for the estimation of the depth of anisotropy using spatial coherency of shear-wave splitting parameters, Computers & Geosciences, 49, 330-333.

Gao, S. S., K. H. Liu, and M. G. Abdelsalam (2010), Seismic anisotropy beneath the Afar Depression and adjacent areas: Implications for mantle flow, J. Geophys. Res., 115, B12330, DOI: 10.1029/2009JB007141.

Gripp, A. E., and R. G. Gordon (2002), Young tracks of hotspots and current plate velocities, Geophys. J. Int., 150, 321-361.

Hatcher, R. D. (2010), The Appalachian orogeny: A brief summary, in From Rodinia to Pangea: The Lithotectonic Record of the Appalachian Region, Geol. Soc. of Am., Boulder, Colo.

Hoffman, P. F. (1988), united plates of America, the birth of a craton: Early Proterozoic assembly and growth in Laurentia, Annu. Rev. Earth Planet. Sci., 16, 543-603.

Holtzman, B. K., D. L. Kohlstedt, M. E. Zimmerman, F. Heidelback, T. Hiraga, and J. Hustoft (2003), Melt segregation and strain partitioning: Implications for seismic anisotropy and mantle flow, Science, 301, 1227-1230.

Hoffman, P. F. (1991), Did the breakout of Laurentia turn Gondwanaland inside-out?, Science, 252, 1409–1412, doi:10.1126/ science.252.5011.1409.

Huang, Z., L. Wang, D. Zhao, N. Mi, M. Xu (2011), Seismic anisotropy and mantle dynamics beneath China, Earth Planet. Sci. Lett., 306, 105-117.

Karato, S., H. Jung, I. Katayama, P. Skemer (2008), Geodynamic significance of the seismic anisotropy of the upper mantle: New insights from laboratory studies, Annu. Rev. Earth Planet. Sci., 36, 59-95.

King, S. D., and D. L. Anderson (1998), Edge-driven convection, Earth Planet. Sci. Lett., 160, 289–296, doi: 10.1016/ S0012-821X (98)00089-2.

King, S. D. (2007), Hotspots and edge-driven convection, Geology, 35, 223–226, doi:10.1130/G23291A.1.

King, S. D., and J. Ritsema (2000), African hot spot volcanism: small-scale convection in the upper mantle beneath cratons, Science, 290(5494), 1137-1140.

Liu, K. H., S. S. Gao, Y. Gao, and J. Wu (2008), Shear wave splitting and mantle flow associated with the deflected slab beneath northeast Asia, J. Geophys. Res.,113, B01305, doi:10.1029/2007JB005178.

Liu, K. H. (2009), NA-SWS-1.1: A uniform database of teleseismic shear-wave splitting measurements for North America, Geochem. Geophys. Geosyst., 10, Q05011, doi:10.1029/2009GC002440.

Liu, K. H., and S. S. Gao (2011), Estimation of the depth of anisotropy using spatial coherency of shear-wave splitting parameters, Bull. Seismo. Soc. Amer., 101, 2153-2161.

Liu, K. H., and S. S. Gao (2013), Making Reliable Shear-Wave Splitting Measurements, Bull. Seismo. Soc. Amer., 103(5), 2680-2693.

Long, M. D., K. G Jackson, and J. F. McNamara (2016), SKS splitting beneath Transportable Array stations in eastern North America and the signature of past lithospheric deformation, Geochem. Geophys. Geosyst.

Long, M. D., M. H. Benoit, M. C. Chapman, and S. D. King (2010), Upper mantle anisotropy and transition zone thickness beneath southeastern North America and implications for mantle dynamics, Geochem. Geophys. Geosyst., 11, Q10012.

Long, M. D., and P. G. Silver (2009), Shear wave splitting anisotropy: Measurements, Interpretation, and new Directions, Survey Geophys., 407-461.

Marone, F., B. Romanowicz (2007), The depth distribution of azimuthal anisotropy in the continental upper mantle, Nature 447, 198–201.

Montagner, J. (1998), Where can seismic anisotropy be detected in the Earth's mantle? In boundary layers ..., Pure Appl. Geophys., 151, 223-256.

Nicolas, A. (1993), Why fast polarization directions of SKS seismic waves are parallel to mountain belts?, Phys. Earth Planet. Int., 78, 337-342.77.

Nicolas, A., and N. I. Christensen (1987), Formation of anisotropy in upper mantle peridotites: A review, in composition structure and Dynamics of the Lithosphere-Asthenosphere System, Geodyn. Ser., 16, 338-343.

Refayee, H. A., B. B. Yang, K. H. Liu, and S. S. Gao (2014), Mantle flow and lithosphere- asthenosphere coupling beneath the southwestern edge of the North American Craton: Constraints from shear-wave splitting measurements, Earth Planet. Sci. Lett., doi: 10.1016/j.epsl.2013.01.031.

Savage, M. K. (1999), Seismic anisotropy and mantle deformation: what we learned from shear-wave splitting, Rev. Geophys., 37, 65-106.

Savage, M. K., and P. G. Silver (1993), Mantle deformation and tectonics: Constraints from seismic anisotropy in western United States, Phys. Earth Planet. In., 78, 207–227.

Silver, P. G., and W. W. Chan (1991), Shear wave splitting and subcontinental mantle deformation, J. Geophys. Res., 96, 16,429–16,454.

Silver, P. G. (1996), Seismic anisotropy beneath the continents: Probing the depths of geology, Annu. Rev. Earth Planet., Sci. 24, 385– 432.

Silver, P. G., and M. Savage (1994), The interpretation of shear-wave splitting parameters in the presence of two anisotropic layers, Geophys. J. Int., 119, 949-963, doi:10.1111/j.1365-246X.1994.tb04027.x.

Silver, P. G., and W. W. Chan (1991), Shear wave splitting and subcontinent mantle deformation, J. Geophys. Res., 96, 16,429-16,454.

Thomas, W. A. (2006), Tectonic inheritance at a continental margin, GSA Today, 16, 4–11, doi: 10.1130/1052-5173(2006)016 2.0.CO; 2.

Van der Lee, S., K. Regenauer-Lieb, and D. A. Yuen (2008), The role of water in connecting past and future episodes of subduction, Earth Planet. Sci. Lett., 273, 15 – 27, doi:10.1016/j.epsl.2008.04.041.

Van der Lee, S., and A. Frederiksen (2005), Surface wave tomography applied to the North America upper mantle, in Seismic Earth: Array Analysis of Broadband Seismograms, Geophys. Monogr. Ser., vol. 157.

Vecsey, L., J. Plomerova, and V. Babuska (2008), Shear-wave splitting measurements—Problems and solutions, Tectonophysics, 462, 178–196.

Wagner, L. S., M. D. Long, M. D. Johnston, and M. H. Benoit (2012), Lithospheric and asthenospheric contributions to shear-wave splitting observations in the southeastern United States, Earth Planet. Sci. Lett., 341-344, 128-138, doi: 10.1016/j.epsl.2012.06.020.

Whitmeyer, S. J. and K. E. Karlstrom (2007), Tectonic model for the Proterozoic growth of North America, Geosphere, 34, 220–259.

Yang, B. B., S. S. Gao, K. H. Liu, A. A. Elsheikh, A. A. Lemnifi, H. A. Refayee, and Y. Yu (2014), Seismic anisotropy and mantle flow beneath the northern Great Plains of North America, J. Geophys. Res. Solid Earth, 119, 1971–1985, doi:10.1002/2013JB010561.

Yuan, H., and B. Romanowicz (2010), Lithospheric layering in the North American craton, Nature, 466, 1063-1069.

Yuan, H., S. French, P. Cupillard, and B. Romanowicz (2014), Lithospheric expression of geological units in central and eastern North America from full waveform tomography, Earth Planet. Sci. Lett., 402, 176-186.

Zhang, S., and S. I. Karato (1995), Lattice preferred orientation of olivine aggregates deformed in simple shear, Nature, 375, 774-777.

VITA

Yunhua Liu was born in Qinghai, a province located in northwestern part of China. In May of 2014, she received her Bachelor's degree in Geology and Geophysics from Missouri University of Science and Technology, and Bachelor's degree in Exploration of Geophysics from China University of Petroleum (Huadong). At the same year, she began the graduate program in Geophysics at the Missouri University of Science and Technology. She received her Master's degree in Geophysics from Missouri University of Science and Technology in July 2016.

During Yunhua's time at Missouri S&T, she was involved in many activities. She taught two geophysical courses during her graduate studies. She was an active member in the Society of Exploration Geophysics, American Geophysical Union (AGU), and American Association of Petroleum Geologist (AAPG).

During her graduate studies, she participated in two academic conference. In March of 2015, she presented her undergraduate student research at the south-central section meeting of GSA in Oklahoma City, Oklahoma. She also presented in the annual meeting of the AGU in December of 2015.

Yunhua was awarded the Clifford Bishop Memorial scholarship for best senior geophysics student in 2013. She worked for Datapages of AAPG in Tulsa, Oklahoma, as a summer intern in 2015.